



Evaluation of sediment connectivity through physically-based erosion modeling of landscape factor at the event scale

Agustín Millares-Valenzuela^{a,*}, Joris P.C. Eekhout^b, Alberto Martínez-Salvador^c, Rafael García-Lorenzo^c, Pedro Pérez-Cutillas^c, Carmelo Conesa-García^c

^a Environmental Fluid Dynamics Group, Andalusian Institute for Earth System Research (IISTA), University of Granada, Avda. del Mediterráneo s/n 18006, Granada, Spain

^b Centre for Applied Soil Science and Biology of the Segura (CEBAS-CSIC), Soil and Water Conservation Research Group, Murcia, Spain

^c University of Murcia, Department of Geography, Murcia, Spain

ARTICLE INFO

Keywords:

Landscape factor
Sediment connectivity
Event scale
physically-based modeling
Structural vs functional connectivity
Uncertainty

ABSTRACT

Understanding erosion and sedimentation processes along the drainage network, from hillslopes to rivers and reservoirs, is essential for water resources management and river restoration. This work proposes a novel dynamic evaluation of landscape factor from modeled runoff and erosion rates from physically-based distributed hydrological modelling, to estimate event-scale sediment connectivity. Four precipitation events of moderate intensity were selected and used for model calibration. The results were used to analyze the temporal variability of connectivity and comparison with indices based on catchment relief or land-uses. Although the headwater areas of the hillslopes presented similar values for all simulated events, a progressive increase in sediment connectivity, proportional to the runoff magnitude of the event, was observed. The variability of the event-scale connectivity index was mainly controlled by parameters related to flow (riverbed roughness, rill erodibility and particle diameter) and less by land use and vegetation cover (cover fraction or interrill erodibility). Although features affecting functional connectivity caused variations between events, the obtained results agreed with indices based on relief as landscape factor. This highlights the important role of structural connectivity represented by the catchment topography. However, the proposed methodology is subject to several sources of uncertainty related to event-scale model calibration, the erosion and transport processes considered and the spatial distribution of runoff. Furthermore, the geomorphological threshold for hillslope and rivers can also affect sediment connectivity, especially along the fluvial system. The results of this work highlight important future challenges in a more dynamic understanding of sediment connectivity river basins.

1. Introduction

Soil loss and sediment transport downstream is an important challenge worldwide. Their impacts on ecosystem services, forest and agricultural productivity, water cycling and quality, among others, are responsible for significant associated cost (Millares and Moñino, 2018; Brardinoni, 2018; Turnbull et al., 2018; Eekhout et al., 2020; Moreno-Llorca et al., 2020). An important challenge arises to assess transport processes along the drainage network, by considering the spatial and temporal variability at the catchment scale, including both hillslopes and fluvial systems. However, these issues are often addressed separately, by subdivision into different subsystems or from different disciplines. The emerging topic of sediment connectivity offers the

opportunity to study erosion and sedimentation processes holistically, with the potential to increase system understanding and improving basin management (Bracken et al. 2015; Najafi et al., 2021).

Sediment connectivity represents the continuity of sediment fluxes throughout the catchment and conditions the actual sediment delivery at its outlet (Fryirs and Brierley, 2001; Lana-Renault, 2007; Cavalli et al 2013; Messenleh et al., 2014; Micheletti and Lane, 2016; Lane et al., 2017; Rainato et al., 2018; Heckmann et al., 2018; Smetanová et al., 2018a; Smetanová et al., 2018b). As a catchment-scale concept, it is very difficult to estimate due to the multitude of factors and processes involved (Harper et al., 2017; Masselink et al., 2017; Turnbull and Wainwright, 2019). However, future global change will affect land uses and hydro-meteorological drivers and, consequently, will have an

* Corresponding author.

E-mail address: mivalag@ugr.es (A. Millares-Valenzuela).

impact on sediment yield, fluvial morphodynamics and sediment connectivity (Lane 2013; Coulthard and Van De Wiel 2017; Millares and Moñino, 2020; Lisenby et al., 2020). More effort in understanding the processes controlling downstream sediment connectivity is therefore still needed.

From a conceptual point of view, sediment connectivity is characterized by the landscape and the hydro-meteorological drivers (Heckmann et al., 2018). While structural connectivity is determined by the arrangement of landscape units and their characteristics, such as topography, land uses, vegetation cover or soil erodibility (Borselli et al., 2008; Cavalli et al., 2013), functional connectivity characterizes the actual transfer of sediment and their associated processes (Wainwright et al., 2011; Bracken et al., 2015; Cossart and Fressard, 2017). In most cases, hydro-meteorological drivers and structural connectivity conditions functional connectivity. In this regard, water discharge and sediment flow recorded at the outlet of a basin represent temporal signatures of both structural and functional connectivity of the sediment upstream (Heckmann et al., 2018). However, spatial analysis of hillslopes and river processes, and their relationship, is needed to get a full understanding of the sediment connectivity.

At the event scale, functional connectivity, is highly dependent on the temporal scale at which the structural properties of the landscape change significantly (Heckman et al 2018). Intense rainfall episodes could condition phases of connection and disconnection within the catchment related to structural and functional components of connectivity (Bracken et al., 2015). In Mediterranean environments, factors such as the spatial heterogeneity of land use, soil and hydraulic properties, settling velocity and transport capacity, greatly control downstream sediment flow and connectivity between hillslopes and fluvial systems (Millares and Moñino, 2018; Millares et al. 2020). In this regard, the use of models allows investigation of structural and functional connectivity, and their relationship with external drivers. However, at the event scale it is still unclear to what extent the modeled information on sediment connectivity allows interpretation of its structural and functional counterparts (Baartman 2020; Heckman et al 2018). Here, an important issue is how impedance to sediment movement downstream is modelled. Distributed and GIS-based indexes summarize this concept into a weighting or landscape factor, estimated from several parameters such as topography, vegetation, soil and land use (Borselli et al., 2008; Cavalli et al., 2013; Persichillo et al., 2018). However, from both a structural and functional point of view, the concept of landscape factor is dynamic, dependent on the forcing agents and linked to the hydrological processes at the event scale. A better knowledge of this factor, and its dynamics, remains necessary for the theoretical development of the processes controlling sediment connectivity.

The objective of this work was to understand the processes that condition sediment connectivity at the event scale in relation with the structural and functional drivers. To this end, sediment connectivity was evaluated using a dynamic landscape factor calculated from physically-based and distributed hydrological modelling of runoff and soil loss at the event scale. This new landscape factor was subsequently used to modify the Index of Connectivity (*IC*) previously proposed by Borselli et al., (2008) and Cavalli et al. (2013), allowing in turn a direct comparison between different connectivity indices. The methodology was applied in a semi-arid and ephemeral river in southern Spain, where the geomorphology and sediment regimes are extremely diverse (Jaeger et al., 2017; Conesa-García, 1995; López-Bermúdez et al., 2000; López-Bermúdez et al., 2002; Fortugno et al., 2017) and sediment connectivity assessment may be especially helpful.

2. Material and methods

2.1. Sediment connectivity assessment

2.1.1. Dynamic estimation of landscape factor

Here we present a new approach to determine sediment connectivity

by using a landscape factor that considers the spatio-temporal variability of runoff and soil loss at the event scale. This factor was assessed from dimensionless maps representing these processes during the event through physically-based and distributed hydrological and soil loss modeling, using the following expressions

$$\sigma_Q = \frac{\sum_{t=0}^{t=T} Q_{avg}}{\sum_{t=0}^{t=T} Q_{max}} \quad (1)$$

and

$$\sigma_E = \frac{\sum_{t=0}^{t=T} E_{avg}}{\sum_{t=0}^{t=T} E_{max}} \quad (2)$$

where σ_Q is the final map representing the spatio-temporal variability of the runoff, Q_{avg} and Q_{max} , are the mean and the maximum modeled runoff ($m^{-3} s^{-1}$), respectively, at each cell for the duration of the event, T , σ_E is the final map representing the spatio-temporal variability of soil loss at the end of the event, E_{avg} and E_{max} , represent the mean and the maximum modeled soil loss ($kg m^{-2}$), respectively, at each cell for the duration of the event T . Finally, the landscape factor, W_{PBHM} , was estimated from

$$W_{PBHM} = \frac{\sigma_Q}{\sigma_E} \quad (3)$$

This expression considers that soil impedance to sediment transport depends on the spatial variability of runoff along the drainage network during the event, and is inversely proportional to the variability of soil loss. That is, a greater variability of erosion rates over the event implies a lower resistance to sediment transport. This factor was subsequently used to estimate the Index of Connectivity determined by considering both upslope and downslope components at each cell, defined as

$$IC = \log_{10} \left(\frac{\bar{WS}\sqrt{A}}{\sum_j \frac{d_j}{W_j S_j}} \right) \quad (4)$$

where IC is the index of connectivity (Borselli et al., 2008), A is the upslope contributing area (m^2), d_j is the length of the flow path along the j th cell downstream to the outlet (m), W_j and S_j ($m m^{-1}$) are respectively the landscape factor and the slope gradient of the j th cell, with \bar{W} and \bar{S} being their upslope average values. The obtained sediment connectivity index, IC_{PBHM} , was compared to the IC proposed by Borselli et al. (2008), IC_{Bor} , from which the landscape factor is based on the spatially distributed USLE (Universal Soil Loss Equation) C-factor, and the IC proposed by Cavalli et al. (2013), IC_{Cav} , from which the landscape factor is based on the terrain surface roughness. The obtained results were analyzed in terms of structural and functional sediment connectivity at the event scale.

2.1.2. Physically-based distributed modelling

The hillslope erosion model used to assess runoff and soil loss is an adaptation of the numerical scheme presented by Millares et al. (2019). The runoff routing model follows the numerical solution given by Jain and Singh (2005) based on finite volume scheme and D8 flow direction method. The model generates, transports, and deposits sediment in each cell of the DEM, with a spatial resolution of 5 m. The model differentiates two groups of cells according to different erosive processes involved: 1) ordinary hillslope cells, where runoff routing and sediment generation, transport, and sedimentation are modeled. The erosion processes within these cells involves two processes: detachment by raindrop impact (i.e. interrill erosion) and detachment by concentrated flow in rills. In this work, the model does not account for gullying or headcut processes. 2) Channel cells, where river bed erosion, transport and sedimentation is considered. The Courant-Friedrichs-Levy (Courant et al., 1928) condition for this explicit scheme was used to adapt each timestep during the simulation.

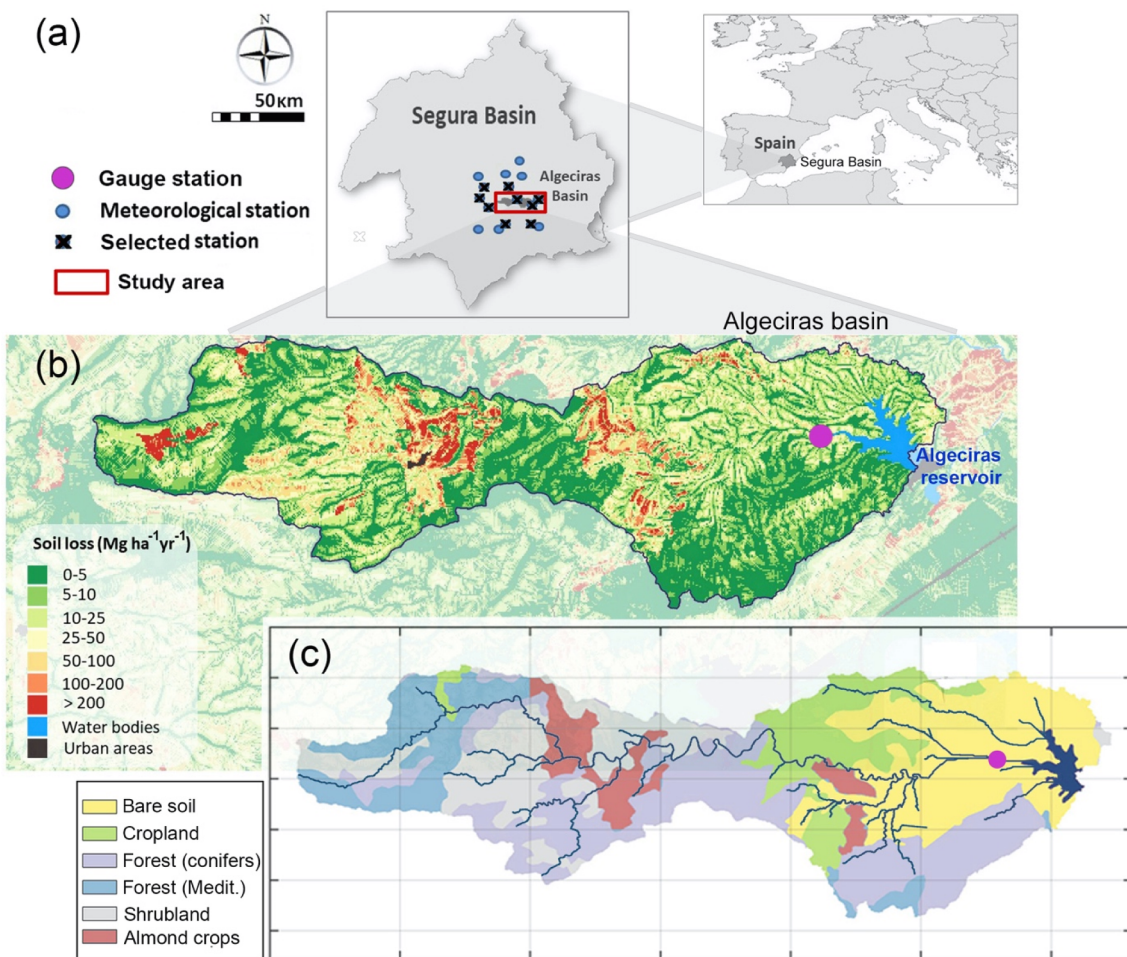


Fig. 1. (a) Location and extension of the Segura Basin and study area; analyzed meteorological stations (blue circles) and selected ones for hydrological modeling (black cross). (b) Location of the Algeciras reservoir, gauge station (magenta circle) and rates of potential soil loss based on the RUSLE model (Dirección General de Medio Natural y Política Forestal, 2007). (c) Distribution of land-uses and drainage network in the study area. (For interpretation of the references to colour in this figure legend, the reader is referred to the web version of this article.)

The soil infiltration, an important process in semi-arid regions (Eekhout et al., 2018), was estimated for each cell from a simplification of the Green-Ampt model (Green and Ampt, 1911, Esteves et al. 2000)

$$I_c = k_s \left[\frac{I_{cum}^t + (h_f + r' \Delta t) \Delta \theta}{I_{cum}^t} \right] \quad (5)$$

where h_f is estimated from the average values of soil texture (Rawls and Brakensiek, 1983), r' is the rainfall intensity ($m s^{-1}$), $\Delta \theta$ is the difference between the saturated and residual soil moisture, I_{cum} and I_c are the accumulated infiltration rate and the infiltration capacity ($m s^{-1}$), respectively, and k_s the soil permeability ($m s^{-1}$). The infiltration rate, i , is calculated from $\min(r', I_c)$ and the accumulated depth at the next time step from $I_{cum}^{t+1} = I_{cum}^t + i' \Delta t$.

The erosion rate due to raindrop processes, D_i ($kg m^{-2} s^{-1}$) on hill-slope cells was calculated from

$$D_i^t = f_c [r']^2 S_{di} K_i \quad (6)$$

where K_i is the interill erodibility ($kg s m^{-4}$), $f_c = 1 - C_f$, being C_f the cover fraction, and S_{di} (Liebenow et al., 1990) is given by:

$$S_{di} = 1.05 - 0.85e^{-4\sin(\alpha)} \quad (7)$$

α being the cell slope gradient. The relative depth of each process of generation and deposition of sediment related to the concentrated flow in rills and channels was obtained from the following

$$h_r^t = \left[\frac{Q_{out}^t}{N_r^t u_r^t} \right]^{1/2} \quad (8)$$

$$h_c^t = \left[\frac{Q_{out}^t n}{S^{0.5} w_c^t} \right]^{3/5} \quad (9)$$

where Q_{out} ($m^3 s^{-1}$) is the modeled runoff of each cell and u_r is the flow velocity in rills, estimated from the empirical relationship $u_r = 3.52(Q_{out}/N_r)^{0.294}$ (Govers, 1992), w_c is the channel width, n is the manning coefficient ($m^{-1/3} s^{-1}$) and S is the cell slope (-). The rill density, N_r^t , was considered variable over time and is a function of the water flow, soil moisture, soil roughness due to tillage practices, slope and surface vegetation cover (Mancilla et al., 2005),

$$N_r^t = W \left[0.66 + 4.14e4 \ln \left(\frac{Q_{out}}{W} \right) + 0.91 \ln(M_o^{t-1}) + 2.04 \ln(S) - 0.37 \ln \left(\frac{Vr}{Rr} \right) \right] \quad (10)$$

Where W is the cell width (m), M_o^{t-1} is the previous soil moisture content in the first 15 cm, $M_o = I_{cum}/0.15$, Vr represents the fraction of plant residue fraction, and Rr is the random soil roughness Mancilla et al. (2005), which was determined from the available land-use and vegetation cover maps (CLC, 2018). The model considers hydraulic sections based on rectangles and isosceles triangles for rills, so the hydraulic radius is obtained from $R_r^t = h_r^t/(2\sqrt{2})$. In channel cells, the

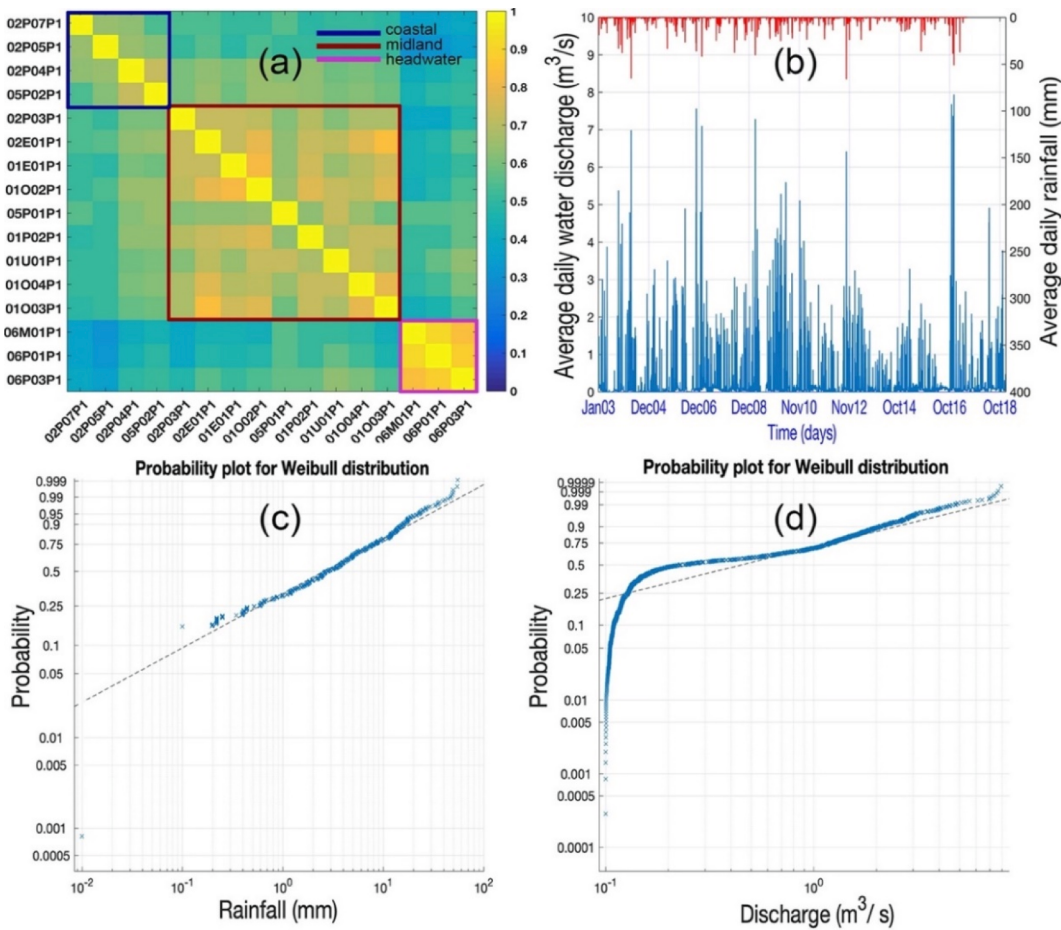


Fig. 2. (a) Correlation matrix of daily precipitation (mm) for the Algeciras basin region by identifying between coastal, midland and headwater stations. (b) Daily precipitation data, as the average of the midland meteorological stations during 2003–2018, and the average daily water discharge estimated at the Algeciras Reservoir. (c) Probability plot for a Weibull distribution function for daily average precipitation at the study site. (d) Probability plot for a Weibull distribution function for the average daily water discharge greater than $0.1 \text{ m}^3/\text{s}$ measured at the Algeciras reservoir.

hydraulic radius is simplified to the water depth, $R_c^t \approx h_c^t$, while the channel width is calculated as

$$w_c = c_1 (Q_{out}^t)^{c_2} \quad (11)$$

Here, the coefficient c_1 and exponent c_2 are 4.02 and 0.44 respectively (Leopold and Maddock, 1953). The erosion/deposition rate for rill processes, D_r ($\text{kg m}^{-2} \text{s}^{-1}$), was calculated from the balance between the rill transport capacity, T_{cr} ($\text{kg s}^{-1} \text{m}^{-1}$), and the sediment load (Yalin, 1963; Nearing et al., 1989), as follows

$$T_{cr}^t = k_T (\tau_r^t)^{1.5} \quad (12)$$

and

$$Q_{sr}^t = \frac{Q_{out}^t}{h_r^t N_r^t}, \quad (13)$$

where $k_T = 0.4433 + 0.2021 \ln(\tau_r^*)$ (Ferro, 1998) and $\tau_r^* = \tau_r^t / [(G - 1)\rho g d_m]$, with g being the gravitational acceleration ($\text{m}^2 \text{s}^{-1}$) and $\tau_r^t = \rho g R_s^t S_{fr}^t$, where $G = \rho_s / \rho$, $\rho = 1000 \text{ kg m}^{-3}$, and $\rho_s = 2650 \text{ kg m}^{-3}$. The factor f_r/f_T represents the relationship between the friction acting on the soil ($f_r = 8gR_s^t u_r^2$) and the total friction: $f_T = 1.11 + 42.76(1 - e^{77.3Rr} + 1.85St + 113.73Vr^3)$ (Gilley and Weltz, 1995). Finally,

$$D_r^t = \begin{cases} K_r (\tau_r^t - \tau_{rc}) (1 - \frac{Q_{sr}^t}{T_{cr}^t}) & \text{for } T_{cr}^t \geq Q_{sr}^t \\ 0.5 \frac{V_s}{q} (T_{cr}^t - Q_{sr}^t) & \text{for } T_{cr}^t < Q_{sr}^t \end{cases} \quad (14)$$

where D_r is the erosion/sedimentation rate within rills ($\text{kg m}^{-2} \text{s}^{-1}$), K_r is the rill erodibility (s m^{-1}), τ_{rc} is the critical shear stress, and Q_{sr} is the sediment load ($\text{kg s}^{-1} \text{m}^{-1}$). The settling velocity, V_s (m s^{-1}), was calculated from

$$V_s = \frac{12\nu_m}{d_m C_D} \left[\left(1 + \frac{C_D d_*^3}{108} \right)^{0.5} - 1 \right] \quad (15)$$

where $C_D = 0.168$, $\nu_m = 1.01 \cdot 10^{-6} \text{ m}^2 \text{s}^{-1}$ and d_* is given by $d_* = d_m [(G - 1)g / \nu_m^2]^{1/3} \nu_m^2$ being the water kinematic viscosity. Detachment corresponding to channels, D_c ($\text{kg m}^{-2} \text{s}^{-1}$), follow the same scheme proposed by equations (12) to (15).

The total erosion/deposition rate in each cell, E^t (kg m^{-2}), corresponds to the sum of the processes considered in the following equation

$$E^t = (A_i D_i + A_r D_r + A_c D_c) dt \quad (16)$$

where A_i , A_r , A_c are the relative areas of interrill, rill and channel zones within the cell for each time of the simulation.

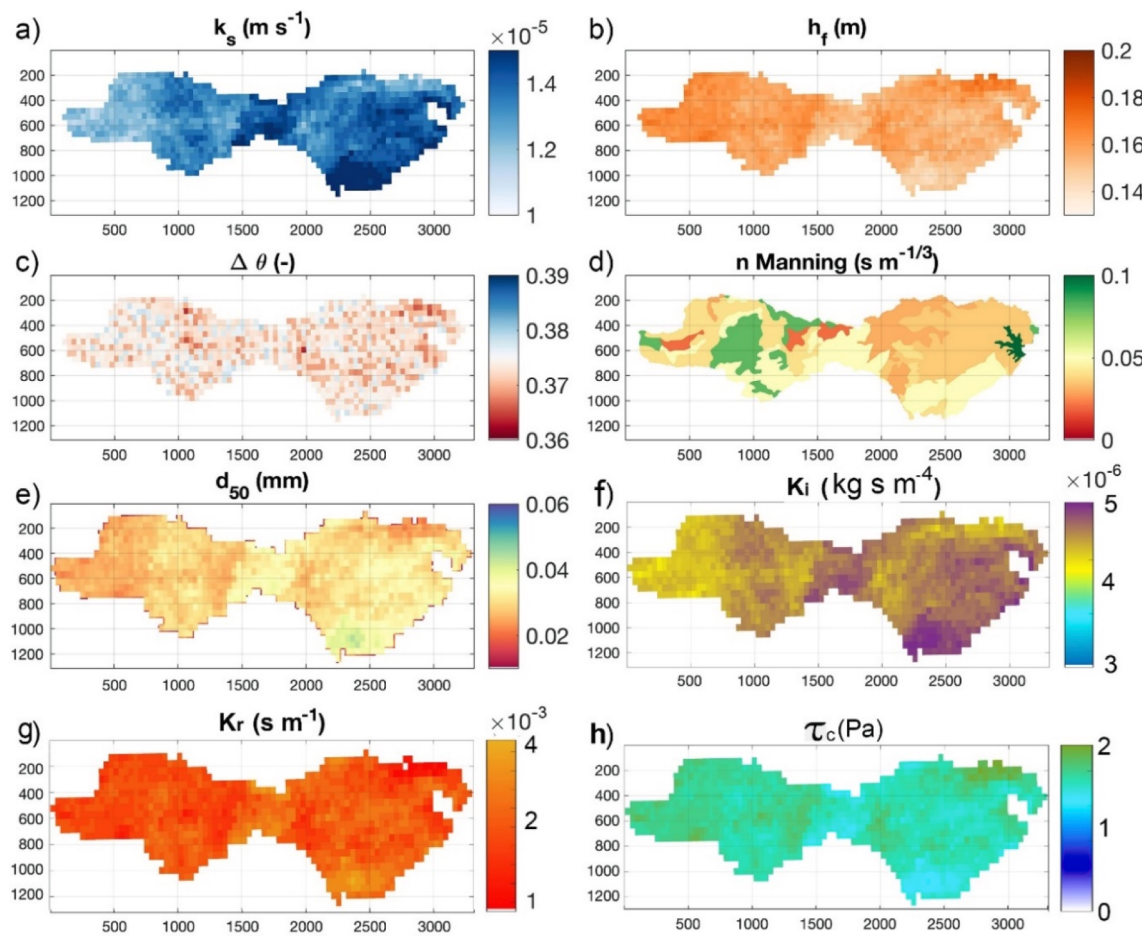


Fig. 3. Distribution of soil and erosion parameters in the study area. (a) Hydraulic conductivity of the soil, (b) wetting front capillary pressure head; (c) dry specific weight of the soil; (d) hillslope Manning's coefficient; (e) estimated soil particle size, (f) estimated interrill erodibility, g) estimated rill erodibility and h) estimated critical shear stress.

Table 1

Summary of the main characteristics of the selected events used.

Event	Date and time	Duration (hours)	Accumulated precipitation (mm)	Max. rain intensity (mm/h)	Q. max. (m ³ /s)	Std (m ³ /s)	Baseflow (m ³ /s)
1	17/08/2010-07:00-17/08/2010-13:00	6	28.8	9.8	7.45	3.2	0
2	11/11/2012-17:00-11/11/2012-00:00	8	23.4	7.3	7.50	3.65	0
3	04/12/2016-16:00-05/12/2016-00:00	8	25.2	8.0	10.55	2.8	2
4	17/12/2016-11:00-17/12/2016-17:00	7	35.8	9.3	11.1	3.33	2.5

2.2. Application

2.2.1. Study site and available data

The proposed sediment connectivity index was estimated in the Segura River basin (southeast of Spain; Fig. 1a), an area with great climatic contrasts, frequent droughts, torrential rains, recurrent floods, high temperatures and heavy frosts (Romero et al., 1992; Grindlay et al., 2011). The selected catchment comprises the Algeciras stream network ($37^{\circ} 53'5\text{N}$; $1^{\circ} 25'20\text{W}$) with a total surface area of 45.9 km^2 . The basin has an elongated geometry, composed of two subareas constricted in the middle with altitudes ranging from 200 to 1,320 m. a.s.l. The catchment is drained by the Rambla de Algeciras, an ephemeral stream that is approximately 15 km in length and a tributary stream of the Guadalentín River. Its pluviometric regime is marked by $<400 \text{ mm}$ of average annual rainfall, great temporal variability with mean coefficient of variation of 0.37, and the occurrence of torrential rainstorms (Martínez-Salvador et al., 2021). In addition, the study area presents a marked

precipitation gradient, with an average annual precipitation of 323 mm at the Algeciras reservoir and 500 mm in the headwaters, located in the Natural Park of Sierra Espuña.

Geologically, this basin belongs to the domain of the Betic and Subbetic units with tertiary sediments, deposited after the emplacement of the Betic mantles. Limestones and dolomites, siliceous marls, and marly limestone outcrops are present in the headwaters, while in the middle and lower parts of the basin marls and alluvial sediments abound, which have favored linear incision, resulting in V-shaped badlands. The associated edaphic profile, of detrital nature composed by little or no cemented loamy soils, marls and polygenic conglomerates, are highly erodible and subject to different dominant erosive processes, such as laminar flow, rilling, piping and gullyling (Hout et al., 2020). At the studied site, previous studies have estimated potential erosion using the RUSLE model (Renard et al., 1991; Dirección General de Medio Natural y Política Forestal, 2007; Fig. 1b). These erosion rates are highly correlated to land use (Fig. 1c), estimated from the Copernicus Land

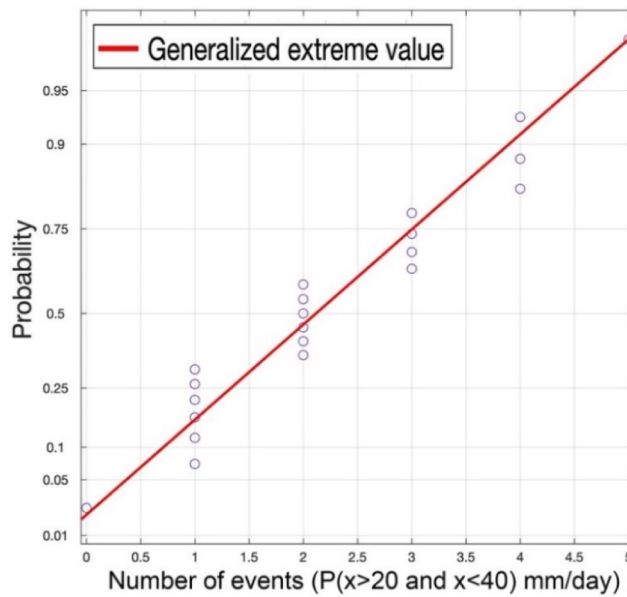


Fig. 4. Probability distribution function of the random variable for the number of annual events between 20 and 40 mm/day, with the fit of a generalized extreme values.

Monitoring Service (CLC, 2018), with values of potential soil loss of 15.3, 2.6, 34.2, 48.7, and 12.3 t ha⁻¹ year⁻¹ for bare soil, forest, almond crops, cropland and shrubland, respectively.

The climatic settings were assessed using the long-term daily precipitation time series from 16 meteorological stations. Fig. 2a shows the correlation for the entire available dataset (2003–2018). A very notable regionalization can be seen, involving groups of stations in the headwaters and mountain zones (lower right corner), the stations in the midlands, and those in the coastal areas (upper left corner), the latter showing lower variability between stations. This analysis highlights the spatial heterogeneity of precipitation in the study area. Nine

meteorological stations with hourly data were selected as input for the hydrological model and to evaluate the spatial distribution of rainfall for the selected events (marked with a black cross in Fig. 1a). For this, an inverse distance weighting (IDW) method was selected to spatially interpolate the precipitation for each required timestep.

Water discharge was estimated from the gauging reports provided by the Hydrographic Studies Center (CEDEX) for the Segura River basin. There is no water level gauge discharge available in the study area, hence, this was estimated from hourly information of the Algeciras reservoir, with the following expression

$$Q_{in_R} = \frac{dV}{dt} + Q_{Out_R} \quad (17)$$

where Q_{in_R} is the estimated inflow to the reservoir (m³/s) from the main stream catchment, dV is the water volume in the reservoir given by the reservoir managers (m³), dt represents the time step (seconds) and Q_{Out_R} is the outflow delivered at the dam, including water extraction from the reservoir, given by the reservoir managers (m³/s). Lateral inputs to the reservoir, evaporation and seepage have been considered negligible with respect to the contribution of the main channel at the event scale. Fig. 2b represents the time series of the estimated mean daily inflow into the Algeciras reservoir (bottom and left axis) and the mean daily precipitation of midland stations (top and right axis). Large variability in the pluviometric regime is observed, with daily events exceeding 50 mm in four occasions and associated responses between 5 to 8 m³/s for the daily mean discharge. Fig. 2c-d show the probability distribution functions for the precipitation time series of the selected stations and for the water discharge measured at the outlet of the basin, respectively. It can be seen that both variables fit well to a Weibull probability distribution for values greater than 0.1 mm of daily precipitation and 0.5 m³/s daily average water discharge. In accordance with this analysis, it is important to note that daily precipitation events greater than 20 mm and 2 m³/s have a probability of occurrence of 10%.

Soil texture data relating to the clay, sand, and silt fractions, as well as the organic matter content and bulk density were supplied by Soil-Grids (Hengl et al., 2017; Soilgrids, 2020) with pixel resolution of 250 m. This information was confirmed with the local edaphic data

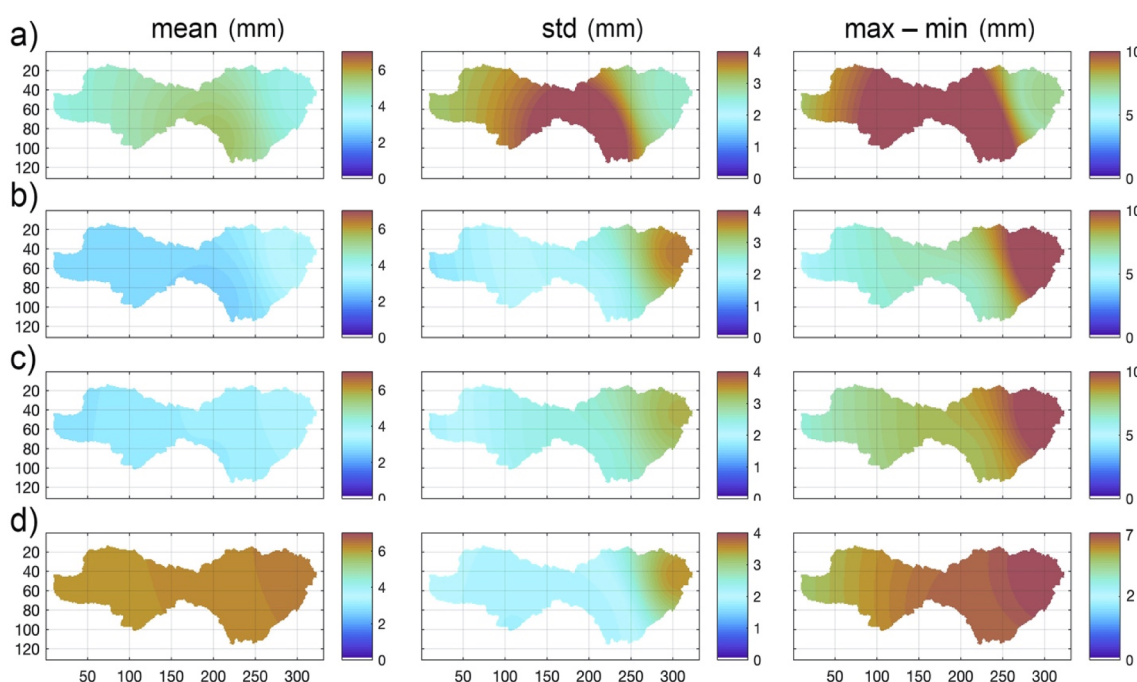


Fig. 5. Spatial distribution of the mean, standard deviation, and maximum and minimum values of precipitation for the selected events (mm). 1 (a), 2 (b), 3 (c) and 4 (d), respectively.

Table 2

Calibration parameters and optimization results for events 1 to 4. The symbol (-) indicates a constant value instead of distributed values. The factor affecting the original maps, the Nash-Sutcliffe model efficiency (NSE), the ratio of the root mean square error and standard deviation of measured data (RSR), the mean relative error (MRE) and the peak error (PE) are also shown.

Event	Parameter	Map factor	Parameter values (mean, max, min)	NSE	RSR	MRE (%)	PE ($\text{m}^3 \text{s}^{-1}$)
1	n_h	0.15	0.015; 0.02; 0.01	0.78	0.056	12	-0.69
	n_{str}	(-)	0.035				
	k_{s-h} (10^{-6} m/s)	0.17	2.29; 2.7; 1.9				
	k_{s-c} (10^{-6} m/s)	(-)	10				
	$h_f(\text{m})$	1	0.0018; 0.0052; 0.0001				
	$\Delta\theta$ (-)	1	0.015; 0.040; 0.001				
2	n_h	0.3	0.014; 0.03; 0.01	0.81	0.044	9	0.92
	n_{str}	(-)	0.035				
	k_{s-h} (10^{-6} m/s)	0.1	0.94; 1.15; 0.78				
	k_{s-c} (10^{-6} m/s)	(-)	10				
	$h_f(\text{m})$	1	0.0018; 0.0052; 0.0001				
	$\Delta\theta$ (-)	1	0.015; 0.040; 0.001				
3	n_h	1.5	0.062; 0.15; 0.03	0.69	0.003	11	-0.57
	n_{str}	(-)	0.035				
	k_{s-h} (10^{-6} m/s)	0.06	0.67; 0.79; 0.55				
	k_{s-c} (10^{-6} m/s)	(-)	10				
	$h_f(\text{m})$	1	0.0018; 0.0052; 0.0001				
	$\Delta\theta$ (-)	1	0.015; 0.040; 0.001				
4	n_h	0.2	0.02; 0.03; 0.01	0.62	0.006	14	-1.25
	n_{str}	(-)	0.035				
	k_{s-h} (10^{-6} m/s)	0.14	1.90; 2.23; 1.56				
	k_{s-c} (10^{-6} m/s)	(-)	10				
	$h_f(\text{m})$	1	0.0018; 0.0052; 0.0001				
	$\Delta\theta$ (-)	1	0.015; 0.040; 0.001				

previously obtained from field campaigns (Rojo et al. 1996) to define raster layers. The topography was defined using a Digital Elevation Model (DEM), with a spatial resolution of 5 m. It was obtained by automatic correlation and digital aerotriangulation of orthophotos, with 25 cm of resolution and ground sample distance of 25 cm, and from the point cloud of the Airborne Laser Scanning surveys carried out within the National Plan for Aerial Orthophotography (PNOA) (CNIG, 2020).

2.2.2. Estimated model parameters

The saturated hydraulic conductivity was determined from pedo-transfer functions (Saxton and Rawls, 2006) as a raster layer with a spatial resolution of 250 m per pixel. Using the soil parameters within hillslopes cells, the values of soil erodibility, K_i , K_r and critical shear stress τ_c were obtained from empirical relationships based on the soil textures, particle diameter, organic matter content and dry specific weight of the soil (Foster et al., 1995; Romero et al., 2007). The geometric sediment diameter on the hillslopes was estimated from the soil texture information, using the model proposed by Shirazi and Boersma (1984). In addition, the analysis of land uses and the vegetation cover map available for the study area (CLC, 2018) revealed great homogeneity in tillage practices, for which constant values of the plant residue and random soil roughness of 0.2 and 0.06 respectively, were considered (Mancilla et al., 2005). The values of the hydraulic roughness parameter were estimated separately for hillslope areas, n_h , based on the values proposed by Engman et al. (1986), Weltz et al. (1992) and Medeiros et al. (2012). Fig. 3 shows the distribution of estimated soil and erosion parameters.

The lack of edaphic information in channel areas limited a more objective estimation of erodibility and critical shear stress for these cells. In this work, a constant value of $K_{channel} = 0.5 \text{ } 10^{-3} \text{ s m}^{-1}$ and $\tau_{c-channel} = 10 \text{ Pa}$ was assumed for greater than 40% of rock fragment content and cohesive soils as previously reported (Knapen et al., 2007; Thoman and Niezgoda, 2008; Niu et al., 2019). The in-stream values of flow resistance, n_{str} , were estimated considering the presence of riparian vegetation (Arcement and Schneider, 1989), with a constant value of 0.043 s $\text{m}^{1/3}$. The USLE-C factor was obtained from the European Cover

Management factor (Panagos et al., 2015). The surface roughness was estimated from the available DEM, a 5x5 moving window and the mean elevation of the 25 surrounding cells, as described by Cavalli et al. (2013).

2.2.3. Event-scale analysis

Event-scale and rainfall-runoff responses are highly variable in Mediterranean regions (Kim and Ivanov, 2014; Merheb et al., 2016; Saffarpour et al., 2016; Smetanová et al., 2018a). At the event timescale, it is important to analyze in detail the annual frequency of events that, presumably, control the annual soil loss in the study area. In this regard, some authors (e.g., Larson et al. 1997) have related the frequency of erosive-dominating events to return periods of around 10 years, which is in line with the probabilistic results found here for precipitation and water discharge.

The selection of the events was based on analyzing and comparing hourly precipitation and discharge records estimated by the water authority of the Algeciras reservoir. We selected 25 events with daily rainfall between 20 and 40 mm for the period between 2004 and 2018. We discarded those events that were affected by measurements errors, such as intermittent and negative values. We finally selected four events in the application of the model. Table 1 shows the main characteristics of the selected events, for both water discharge and precipitation.

2.2.4. Model calibration

The runoff calibration was carried out using an iterative process. This involves the use of a factor that modifies the distributed values of the most sensitive hydraulic parameters according to Millares et al (2019): hydraulic roughness on the hillslope, n_h , hydraulic roughness in the stream, n_c , saturated hydraulic conductivity of the soil on the hillslopes, k_{s-h} , saturated hydraulic conductivity of the soil in the stream, k_{s-c} , the wetting front of the pressure head, h_f , and the differences between residual moisture and saturation moisture, $\Delta\theta$. In each iteration, the simulated water discharge at the outlet of the basin was compared with that estimated discharge from Eq. (17) for each selected event. The peak error (PE), the Nash-Sutcliffe model efficiency (NSE), the ratio of the root mean square error and standard deviation of measured data (RSR),

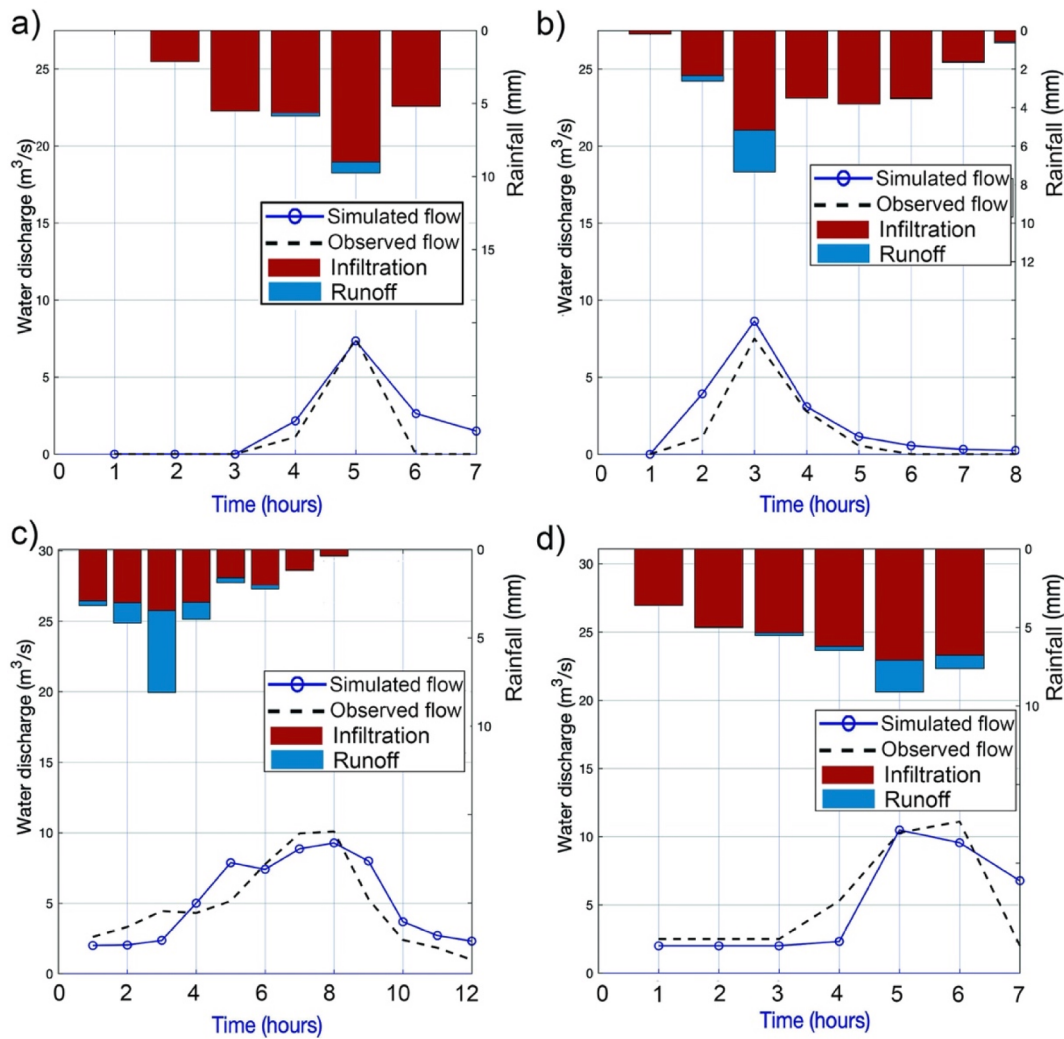


Fig. 6. Results of the calibration of events calibration. Measured hydrograph (black dashed line, left axis), simulated hydrograph (blue circle marked line, left axis), simulated infiltration (red bars, top and right axes) and runoff (blue bars, top and right axes). (For interpretation of the references to colour in this figure legend, the reader is referred to the web version of this article.)

and the mean relative error (MRE) of each simulation, were evaluated as standard goodness of fit of hydrological models (Kalantari et al., 2015; Moriasi et al., 2015).

The modeled soil loss on hillslopes was compared with plot-scale data valid for Mediterranean regions from Maetens et al., (2012), characterized by experimental plot lengths up to 200 m and slope gradient between 4 and 80%, and from Cerdan et al., (2010), characterized by experimental plot length up to 100 m and slope gradient between 4 and 30%. These works assess annual erosive rates, so the erosive effect of each selected event was estimated from the recurrence and the associated probability of the events. Fig. 4 shows the probability distribution function for the number of annual events with precipitation between 20 and 40 mm/day. As observed, the random variable fits well to a generalized extreme value probability function with a mean value of 2.1. This analysis allows us to estimate a value of 2 events per year for the selected events and therefore to relate erosion rates at the event scale to annual rates estimated with other methodologies.

The erosion rate calibration was also carried out using an iterative process, with a factor that modifies the distributed maps of K_r , K_i , and τ_c which are considered to be the most sensitive model parameters and generate the greatest degree of uncertainty, as discussed in Millares et al. (2019). The modeled results were analyzed up to a slope length of 200 m, to allow comparison with previously mentioned work. The final maps

modeled for rill and raindrop erosion at the hillslopes (first and second term in Eq. (16)) were also analyzed separately to estimate the ratio between these two erosive processes.

2.3. Sensitivity and uncertainty analysis

To evaluate the sensitivity of the new landscape factor, and its impacts on sediment connectivity, an iterative simulation procedure was carried out by changing the distributed values of rill and interrill erodibility parameters: sediment particle size, critical shear stress, hillslope and channel roughness and the coverage factor, i.e. the model parameters that could significantly affect the resulting IC_{PBHM} . The sensitivity index SI (dimensionless), was calculated for each incremental change of a given parameter and obtained from the following expression (Van Griensven et al., 2006)

$$SI = \frac{\frac{R_m(p_1, \dots, p_i + \Delta p_i, \dots, p_m) - R_m(p_1, \dots, p_i, \dots, p_m)}{R_m(p_1, \dots, p_i, \dots, p_m)}}{\frac{\Delta p_i}{p_i}} \quad (18)$$

where R_m is the result obtained for IC_{PBHM} and Δp_i is the change in a given parameter p_i , while the remaining parameters are kept constants. The value of Δp_i was changed for the selected parameters by a factor of 0.1 to 5, with incremental steps of 0.1. The sign of SI indicates whether

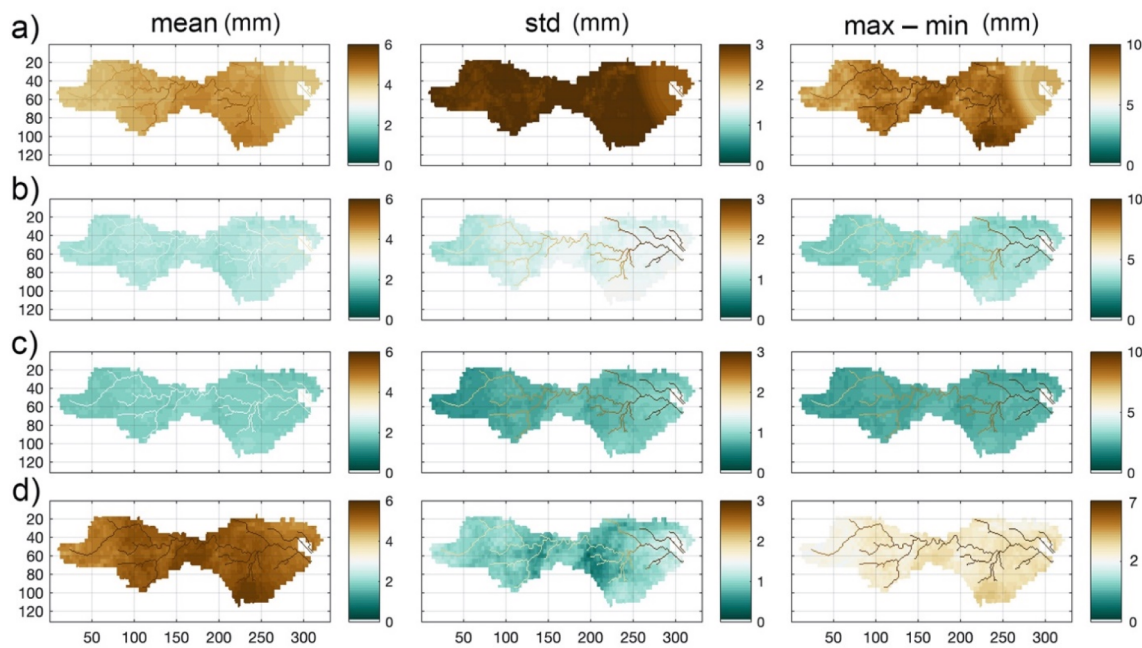


Fig. 7. Distribution of the modeled mean, standard deviation, and maximum and minimum values of infiltration of the selected events, 1 (a), 2 (b), 3 (c), and 4 (d), respectively.

Table 3

Soil loss ($\text{Mg ha}^{-1} \text{yr}^{-1}$) estimated by physically-based modeling and reported by Cerdan et al (2010) and Maetens et al., (2012), for different land-use categories. The values in parentheses indicate the ratio between the modeled raindrop and rill erosion.

t/(ha year)	Bare soil	Forest	Tree crops	Cropland	Shrubland	Mean (L < 200 m)
Physically-based modelling (*)	2.59 (43/57)	0.31 (23/77)	1.83 (27/73)	0.55 (30/70)	0.13 (25/75)	0.94
Cerdan et al. (2010) (**)	9.05	0.18	1.67	0.84	0.54	2.81
Maetens et al. (2012) (***)	3	0.20	0.8	1	0.5	1.08

(*) Calculated by considering two events/year and slope length up to 200 m. The values shown here are the average of the 4 selected events.

(**) Based on short to medium-term soil loss measurements on Mediterranean plots.

(***) Based on the estimated median for a 250–300 mm/year annual precipitation environment.

the index of connectivity responds codirectionally to p_i . For this, 50 simulations were carried out, obtaining SI and averaged IC_{PBHM} values separately for the hillslope and channel areas.

The uncertainty related to the large number of parameters, constraints and adopted assumptions was also assessed. For this purpose, stochastic simulations were performed to evaluate:

a) The uncertainty associated with the rate of soil loss due to the limitations related to the calibration of erosive processes at the event scale. For this, maps and constants of erosion parameters corresponding to K_i , K_r , τ_c , $K_{channel}$, $\tau_{c_channel}$, V_r and R_r were independently affected at each simulation (over 500 simulations) by a factor following a normal probability distribution function with parameters $\mu = 1$ and $\sigma^2 = 0.25$. In addition, the annual number of medium-

magnitude events, between 20 and 40 mm of precipitation, was considered from their fitted probability of occurrence.

b) The uncertainty associated with the geomorphological threshold that separates hillslope and channel cells. This threshold affects both the modeling process and the estimated values for connectivity assessment. For this purpose, 500 simulations were performed by varying the threshold separating hillslopes and streams from a normal distribution of parameters $\mu = 600 \text{ ha}$ and $\sigma^2 = 300 \text{ ha}$.

The results were assessed separately for the mean value of the annual erosion rates for slope lengths < 200 m, its spatial standard deviation and the mean values and standard deviation of IC_{PBHM} for hillslopes and rivers.

3. Results

3.1. Model calibration and event scale analysis

The selected events were calibrated according to the spatial distribution of the forcing agents and the related hydrological processes. Fig. 5 shows the spatial variability of precipitation in each of the events, as the mean, standard deviation, and maximum and minimum values throughout the period of occurrence of the event. The events were grouped according to their magnitude and their spatial distribution. Events 1 and 4, are characterized by a higher rainfall magnitude and have a more homogeneous spatial distribution of precipitation in their maximum values. Events 2 and 3, are characterized by a lower rainfall magnitude and have a more heterogeneous spatial distribution, where maximum precipitation is higher at the catchment outlet.

Table 2 shows the optimal values found during the calibration process for each of the hydraulic parameters considered. The model performance indicators showed satisfactory to very satisfactory values based on the model performance indices used (Moriasi et al., 2007; Kalantari et al., 2015). As shown, there is great variability in the magnitude of the roughness and saturated conductivity on the hillslope, which are considered very sensitive model parameters, as previously reported by Millares et al. (2019). In this regard, events 1 and 4 are considered similar, with calibrated values within the same range. Event 2, differs from these two events with higher values for hillslope

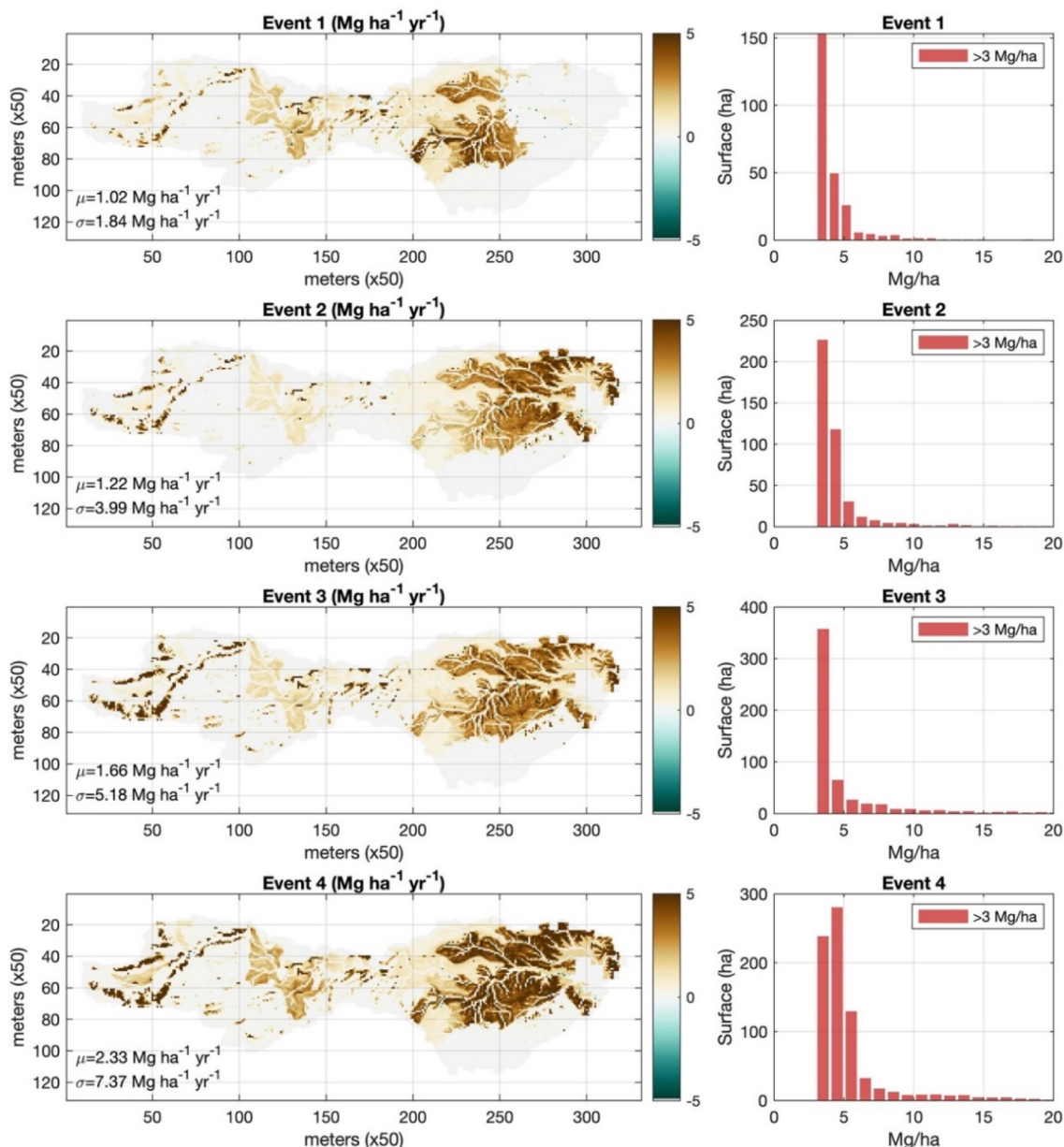


Fig. 8. Distributed annual erosion rates obtained for each selected event. Mean values and standard deviation of erosion rates for slope length < 200 m are shown in each map. Values higher than 3 Mg/ha are analyzed in a separate histogram. Negative values indicate sedimentation.

roughness and lower values for hillslope saturated conductivity. The calibrated parameters for event 3 differ from the other three events, with higher values for roughness and lower values for saturated soil conductivity.

Fig. 6a-d shows the observed and simulated results of water discharge, mean precipitation, and infiltration, estimated from the distributed hourly maps. A differentiated temporal pattern is observed for the mean value of soil infiltration. Events 2 and 3 generate runoff within one and two hours after the start of the event, respectively. On the other hand, for events 1 and 4, the initial period is characterized by infiltration processes and significant runoff occurs from four hours after the start of the event. This highlights the temporal differences in runoff between the analyzed events, in particular for event 3, which is characterized by more continuous runoff. This variability is also reflected in important differences in the spatial distribution of infiltration. Fig. 7 shows the mean, standard deviation, and maximum and minimum values of the infiltration (mm). An important contrast can be appreciated between events 1 and 4 (Fig. 7a,d), and events 2 and 3 (Fig. 7b,c),

and between hillslopes and stream as well. It is remarkable that event 3 presents the lowest distributed values, especially in terms of variability.

For the erosion sub-model we obtained the following factor values after calibration 0.5, 0.1 and 2.3, for the parameters K_r , K_i , and τ_c , respectively. Table 3 shows the mean annual erosion rates obtained by assuming two events per year and for slope lengths up to 200 m. The values are organized by the different land use classes and the ratio between raindrop and rill erosion is shown, as well. As observed, the modeled results are in line with the experimental values obtained by Cerdan et al., (2010) and Maetens et al. (2012). Differences are only observed in scrublands, where the modeled results underestimate the values proposed by these authors. Cerdan et al (2010) show considerable higher values for bare soil although this value is accompanied by a large variability ($\text{std} = 35.23 \text{ Mg ha}^{-1} \text{yr}^{-1}$), as reported by the authors. The ratio between rill and raindrops erosion shows values that ranges between 1:1 and 1:3, which is in line with previous observations (Morgan, 2005; Liu et al., 2011; Xiao et al., 2017).

Fig. 8 shows the soil loss modeled for each event. Both the

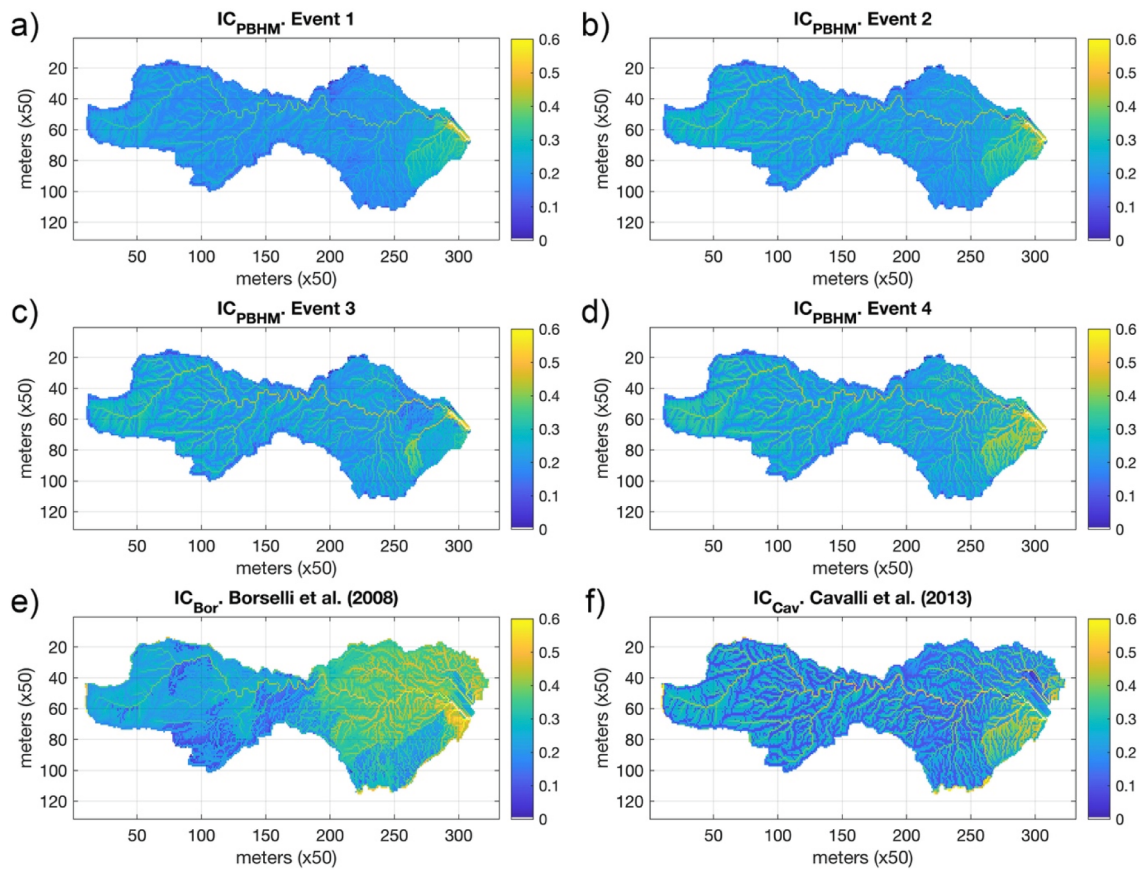


Fig. 9. Distributed results of the connectivity index IC_{PBHM} , IC_{Bor} and IC_{Cav} . Estimations made by physically-based hydrological modeling for events 1, 2, 3, and 4 landscape factor assessment (a, b, c, and d, respectively). Estimations by considering the USLE-C map (Borselli et al., 2008) and the watershed surface relief (Cavalli et al., 2013) as landscape factors (e, f, respectively).

distribution and order of magnitude of values modeled for each of the four events are very similar, with slightly higher values for event 4, visible above all in the central part of the study area, which is dominated by tree crops. Event 1, however, has values that are very low or zero on the bare soil surfaces near the basin outlet due to the low rainfall recorded during the event, which underlines the importance of the spatial distribution of rainfall.

3.2. Sediment connectivity assessment

3.2.1. Event-scale analysis

Fig. 9a-d shows the spatial distribution of IC_{PBHM} for the 4 selected events. Also, the distributed results of methods proposed by Borselli et al., (2008), IC_{Bor} and Cavalli et al., (2013), IC_{Cav} are shown (Fig. 9e-f). As observed, sediment connectivity presents considerable differences among the simulated events. These results can be quantitatively analyzed using the histograms for hillslope and streams cells (Fig. 10). The distribution of IC_{PBHM} on hillslopes can be estimated in all cases from a bimodal distribution which separates the upper areas (up to an accumulated area of 2 ha) from the remaining cells of the hillslope (Fig. 10 a-d). Table 4 summarize the mean values for different locations of hillslopes and fluvial systems. Events 1 to 4 showed a constant value of 0.19 at the upper hillslopes for all events while a progressive mean increasing values were found for IC_{PBHM} downstream. Event 1, with a considerably greater infiltration processes, presented a greater overlap between these two areas as shown in Fig. 10 a.

At the fluvial system a bimodal distribution can also be observed separating the upper stretches of rivers, from those located downstream with cumulative flow greater than 30 km^2 . In this case, a progressive increase of IC_{PBHM} is observed for the modeled events in both areas.

3.2.2. Static vs dynamic landscape factor approaches

The spatial distribution of IC_{PBHM} for events 1 to 4 is comparable with the methodologies proposed by Borselli et al., (2008) and Cavalli et al., (2013). However, the influence of the land-uses cover as landscape factor proposed by Borselli et al., (2008) increases the spatial differences of IC_{Bor} compared to IC_{Cav} and IC_{PBHM} as observed in Fig. 9e and Fig. 10e. By contrast, the model of Cavalli et al., (2013), which depends exclusively on watershed relief, shows clear similarities with IC_{PBHM} , especially for event 4, which is characterized by higher runoff rates (Fig. 10f).

Fig. 11 better illustrates the differences between the dynamic (i.e. IC_{PBHM}) and static assessments (i.e. IC_{Bor} and IC_{Cav}) of landscape factor for the hillslopes and river systems separately. There seems to be a high correlation between IC_{PBHM} and IC_{Cav} for rivers for lower IC values (up to 0.45; Fig. 11a). Event 3, 2 and 1 progressively show lower values of IC_{PBHM} with respect to IC_{Cav} . On the hillslopes (Fig. 11b), the similarity between event 4 is remarkable, while events 1 to 3 presented a more scattered relationship. Regarding IC_{PBHM} and IC_{Bor} , certain linear correlation could be observed at the fluvial system (Fig. 11c) which could be related to the dependency of runoff and soil loss on land use. On the hillslopes, this relationship is much more disperse (Fig. 11d).

3.2.3. Sensitivity and uncertainty assessment

The sensitivity analysis performed suggest a low variability of IC_{PBHM} with respect to the evaluated parameters. Fig. 12 shows the results of 500 simulations for variations in mean particle diameter, rill erodibility, critical shear stress, interrill erodibility, Manning's hillslope and river flow resistance, and cover factor. As observed, the dimensionless value of the highest sensitivity index, SI , is obtained for the roughness of the soil, both on hillslopes and in the streams systems (Fig. 12 a-b). In most

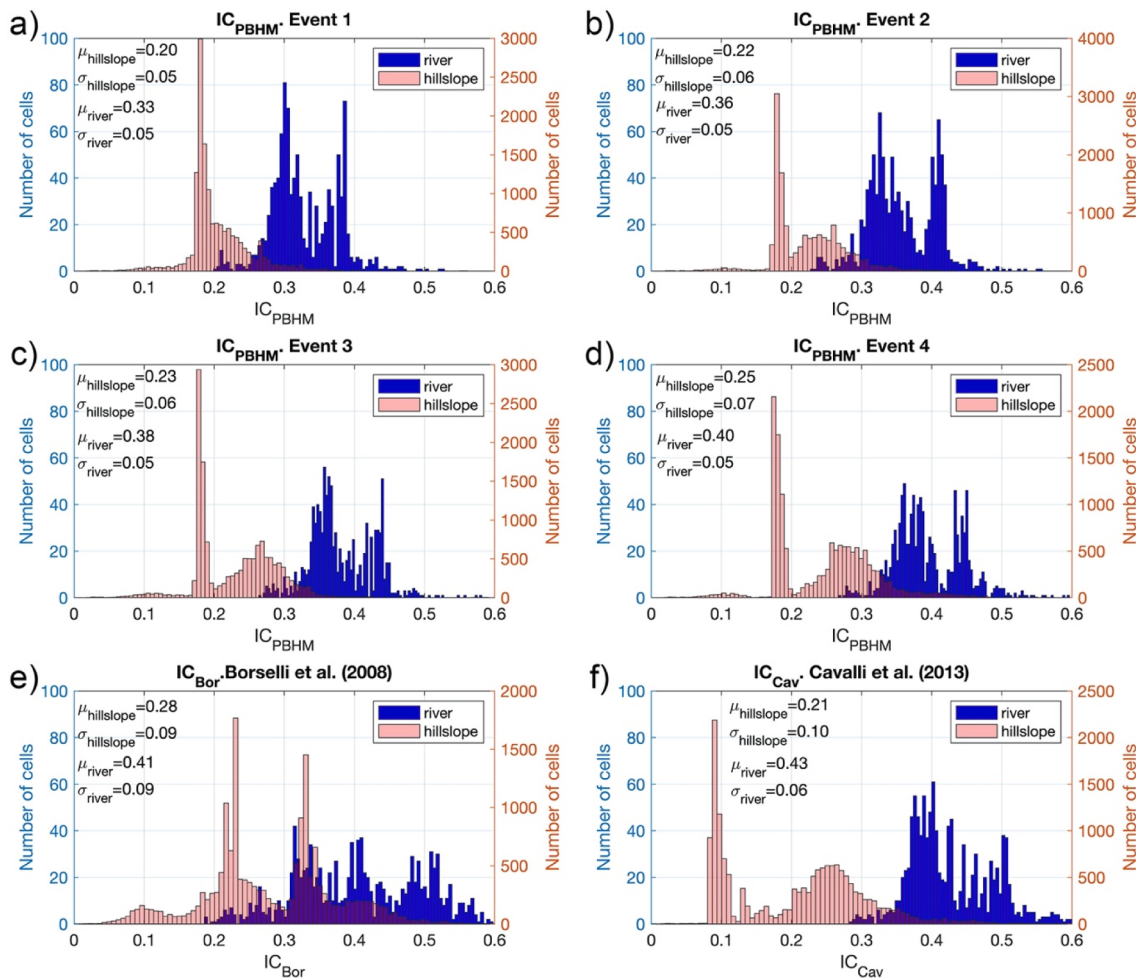


Fig. 10. Histograms of IC_{PBHM} , IC_{Bor} and IC_{Cav} at hillslopes and stream systems. Estimations made by physically-based hydrological modeling for events 1, 2, 3, and 4 for the landscape factor assessment (a, b, c, and d, respectively). Estimations by considering the USLE-C (Borselli et al., 2008) and the watershed relief (Cavalli et al., 2013) as landscape factors (e, f, respectively). Mean and standard deviation is shown separately for hillslopes and rivers.

Table 4

Mean values of IC_{PBHM} , IC_{Bor} , IC_{Cav} for different locations within hillslopes and stream systems. (U.L. Unclear limits).

IC	Upper hillslopes (< 2 ha)	Lower hillslopes (greater than 2 ha)	Upper stream (< 3000 ha)	Lower stream (greater than 3000 ha)
IC_{PBHM}	Event 1	0.19	0.22	0.30
	Event 2	0.19	0.25	0.33
	Event 3	0.19	0.27	0.35
	Event 4	0.19	0.29	0.38
	IC_{Bor}	0.21	0.32	U.L.
IC_{Cav}	0.1	0.25	0.4	0.5

cases, the character of codirectionality (positive values of SI) implies that an increase in flow resistance leads to greater sediment connectivity due to an increase of transport capacity. To a lesser extent, the mean particle diameter, d_m , influences the connectivity of the sediment both on hillslopes and in the streams. Although an increase of d_m would be expected to lead to higher settling velocity, lower transport capacity and higher sedimentation, the balance between transport capacity and the modeled sediment flow causes a highly varied response. In this case, the

lack of codirectionality of SI highlights the non-linear character in the response of the modeled sediment flow. Rill erodibility also seem to lead to important variations in IC_{PBHM} at both hillslopes and streams systems (Fig. 12c and 12d respectively). Interrill erodibility, coverage factor, and critical shear stress do not seem to affect sediment connectivity much.

Regarding uncertainty, Fig. 13 shows the results of the 500 stochastic simulations for the assessment of the annual soil loss (Fig. 13 a-b) and IC_{PBHM} values for hillslopes and rivers (Fig. 13 c-d) of event 1. The empirical probability functions and the best fit of theoretical functions; generalized extreme value (GEV) and extreme value (EV), are also presented. As shown in Fig. 13a, the mean value of the annual rate for slopes up to 200 m is similar, slightly higher than the mean rate estimated for this event (shown in Fig. 8). The spatial variability, estimated at $\sigma = 1.8 \text{ Mg ha}^{-1} \text{ yr}^{-1}$ is slightly further away from the most likely adjusted result, when the variability of erosion-related parameters and the occurrence of the number of annual events are taken into account. These results point to the fact that, although modeled soil loss seems to correctly represent the average conditions of the study area, both the erosion rates and their spatial distribution could be more than twice or five times as high, with a probability of 15 and 19 %, respectively. Here, it is important to note that IC_{PBHM} did not present significant variations due to its dimensionless nature (Eq. (16)).

The uncertainty related to the threshold determining hillslopes and rivers presents a greater impact on IC_{PBHM} , especially in the fluvial system (Fig. 13c, d).

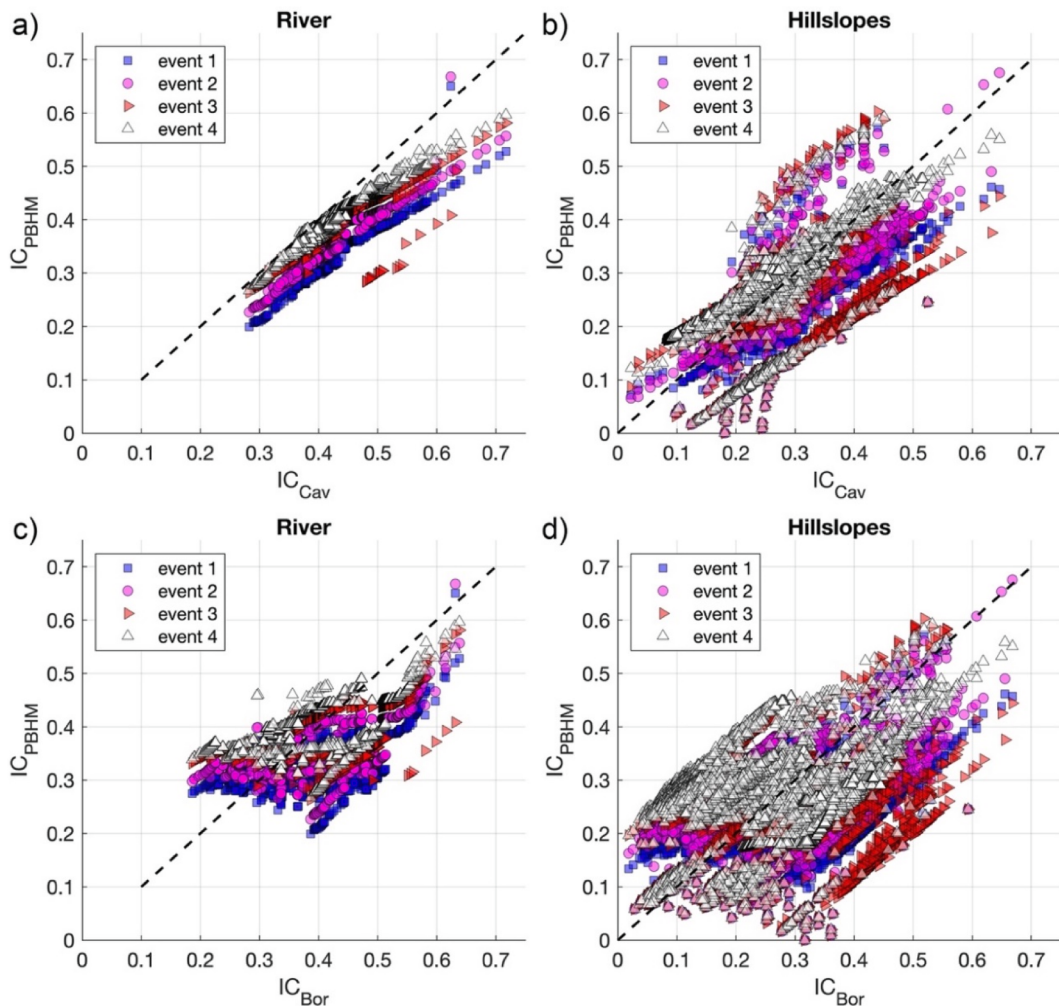


Fig. 11. Relationship between IC_{PBHM} and IC_{Cav} , (a-b), and between IC_{PBHM} and C_{Bor} (c-d) at river and hillslopes systems for the 4 selected events.

4. Discussion

4.1. Variability of sediment connectivity at the event scale

The results showed clear differences in sediment connectivity at the event-scale, for both hillslopes and streams, by considering runoff and erosion processes from dynamic assessment of the landscape factor. The constant value of connectivity at the top of the hillslopes could be explained by the low runoff in these areas (<2 ha). Sediment connectivity increases downstream, from the lower hillslopes to the fluvial system, which is directly proportional to the increase in runoff rates. Furthermore, regarding the sensitivity analysis performed, model parameters affecting water and sediment fluxes, such as flow resistance and rill erodibility, control important variations of sediment connectivity when compared to factors such as land use or interrill erodibility, which do not directly influence these fluxes. From a perspective of the structural and functional components of connectivity, a certain similarity could be found between IC_{PBHM} and IC_{Cav} (Fig. 11 a-b). This similarity is more evident for higher runoff rates (event 4), which highlights the relationship between surface roughness and hydrological processes from static and dynamic assessments of the landscape factors, respectively. Events 1, 2, and 3 show a lower degree of correlation between IC_{PBHM} and IC_{Cav} . Although events 3 and 4 are very similar in terms of runoff magnitude, the hydrological response is faster in event 4, with greater infiltration and runoff processes in less time, which in turn leads to higher soil loss rates for event 4. In this regard, it is important to

highlight the relationship of IC_{PBHM} and the pre-event soil conditions among the selected events, especially for the event 1, which is characterized by higher infiltration rates. These results are in line with previous estimates of sediment connectivity in low-relief catchments (Gay et al., 2016; Hooke et al., 2017; Kalantari et al., 2017), which highlighted the important role of infiltration and runoff processes.

Alternatively, an evaluation of the landscape factor through the variability of sediment fluxes was also carried out. For this, the dimensionless value was calculated from $W_{PBHM} = Qs_{avg}/Qs_{max}$, where Qs_{avg} and Qs_{max} are the average and maximum sediment flow in each cell (Kg s^{-1}). Although this hypothesis has not been compared with measurements in the current study, the results also highlighted the relationship between the magnitude of runoff and sediment connectivity, although with greater relevance to event duration and infiltration processes. This was emphasized in event 3, with longer runoff processes and discharge peaks more distributed over time, which showed lower I_{PBHM} values than the others events both on hillslopes and in streams.

From these results it could be argued that while topography, as intrinsic structural property, can provide a first approximate assessment of sediment connectivity, different hydrological processes between events could greatly modify these values, especially within hillslopes and, to a lesser extent along the fluvial system. It is important to remark that slope is included in the estimation of sediment connectivity through Eq. (4) and in the estimation of the landscape factor, in which the slope is an important parameter in the calculation of runoff, raindrop impact and rilling. Hence, slope is accounted for twice by the proposed method

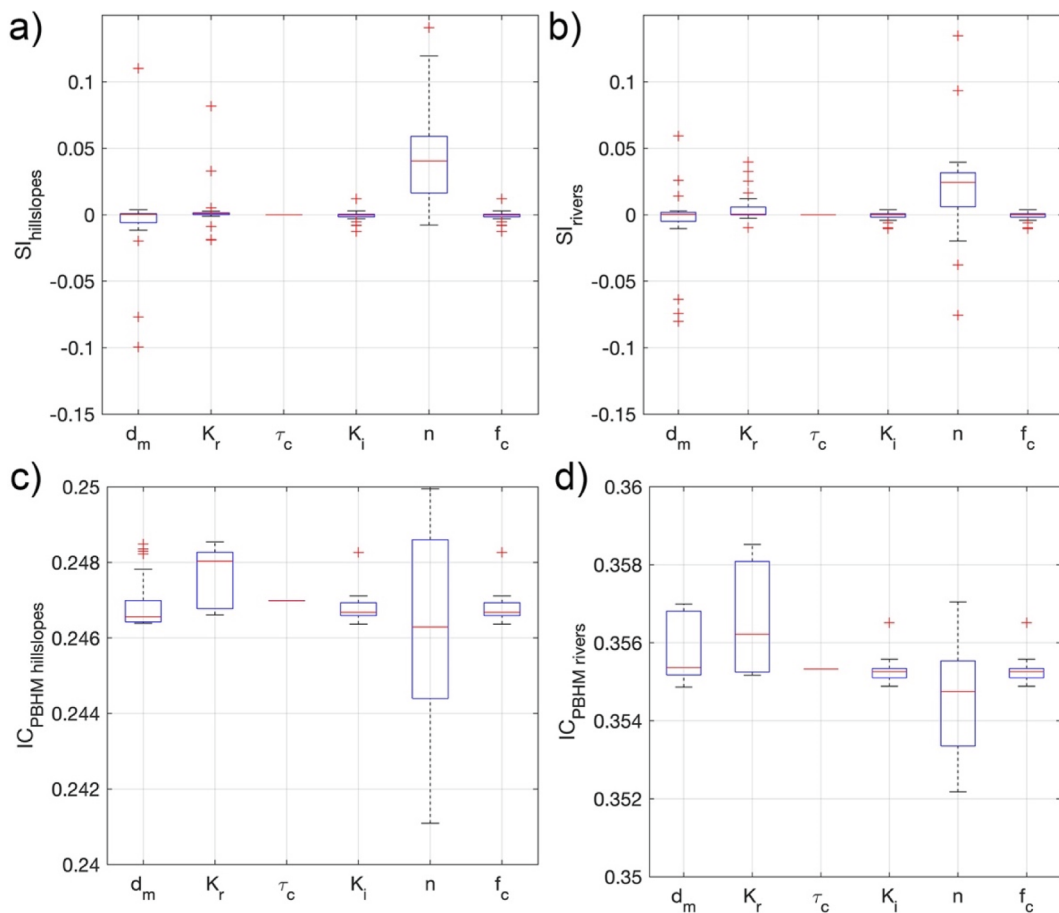


Fig. 12. Sensitivity index SI (a, b) and IC_{PBHM} values (c, d) as affected by different distributed parameters; particle diameter d_m , rill erodibility, K_r , critical shear stress, τ_c , interill erodibility, K_i , hillslope and stream Manning roughness, n_h and n_{str} , respectively, and the cover factor, f_c . Lines, markers and colors represent the medians (red lines), 25th and 75th percentiles (box edges) and extreme data points. (For interpretation of the references to colour in this figure legend, the reader is referred to the web version of this article.)

being difficult to identify the effect of its overlapping. However, this approach allows the evaluation of topography and relief on both structural and functional sediment connectivity.

4.2. Limitations and future research

The obtained results are subject to limitations that condition both potential applications and future research regarding sediment connectivity at the event scale. The relative nature of the proposed landscape factor assessment could give similar impedance classification for high and low variability of runoff and erosion rate simultaneously. Besides, the runoff processes were calibrated at the outlet of the study area, so that the specific infiltration and runoff conditions for hillslopes and channels could not be validated. In this regard, although the modeled values of erosion rates are in line with previous estimations for different land use, no measurements of sediment flow along the drainage were available. Also, the eventual mismatch between the high temporal resolution in modeling tasks (with timestep around 2 s) and the low hourly resolution available for precipitation, could affect both magnitude and distribution of the landscape factor. These limitations, frequent in the calibration and analysis of distributed hydrological models (Merritt et al. 2003), can be important here when analyzing sediment connectivity. It is also important to point out the limitations related to the intensity of the analyzed events that do not represent the extreme events characteristic of Mediterranean areas. These types of events, although infrequent, play a fundamental role in the processes of erosion, transport and sedimentation and, therefore, in sediment connectivity. In addition,

intense events are linked to erosive processes that have not been considered in this study such as gullying, mass failure or debris flows, which could be dominant in some cases (Simon et al., 2000; Thomas et al., 2004).

These limitations should be seen as a motivation for future potential research and applications in other basins. The spatio-temporal variability of the sediment connectivity found between events gives the potential to apply the dynamic approach developed in areas with large heterogeneity in hydro-meteorological forcing, such as other Mediterranean basins or mountain environments. For this, it could be interesting to increase understanding on the physical nature of the processes involved on sediment connectivity, such as snow dynamics, an increased detail in sediment transport processes, such as suspended, bedload and debris flow, and a greater variability of events, including more extreme episodes. These aspects pose a challenge in data collection, both in quality and quantity, including more accurate estimation of fluxes (water and sediment) and erosion rates. The current needs for knowledge on sediment connectivity justifies an increase in institutional efforts in this regard in relation to the important future challenges linked to global change.

5. Conclusions

This work presents a new approach to assess sediment connectivity by dynamically estimating the landscape factor from physically-based and distributed modeling of runoff and soil loss at event-scale. The results have allowed a comparison with estimates of the landscape factor

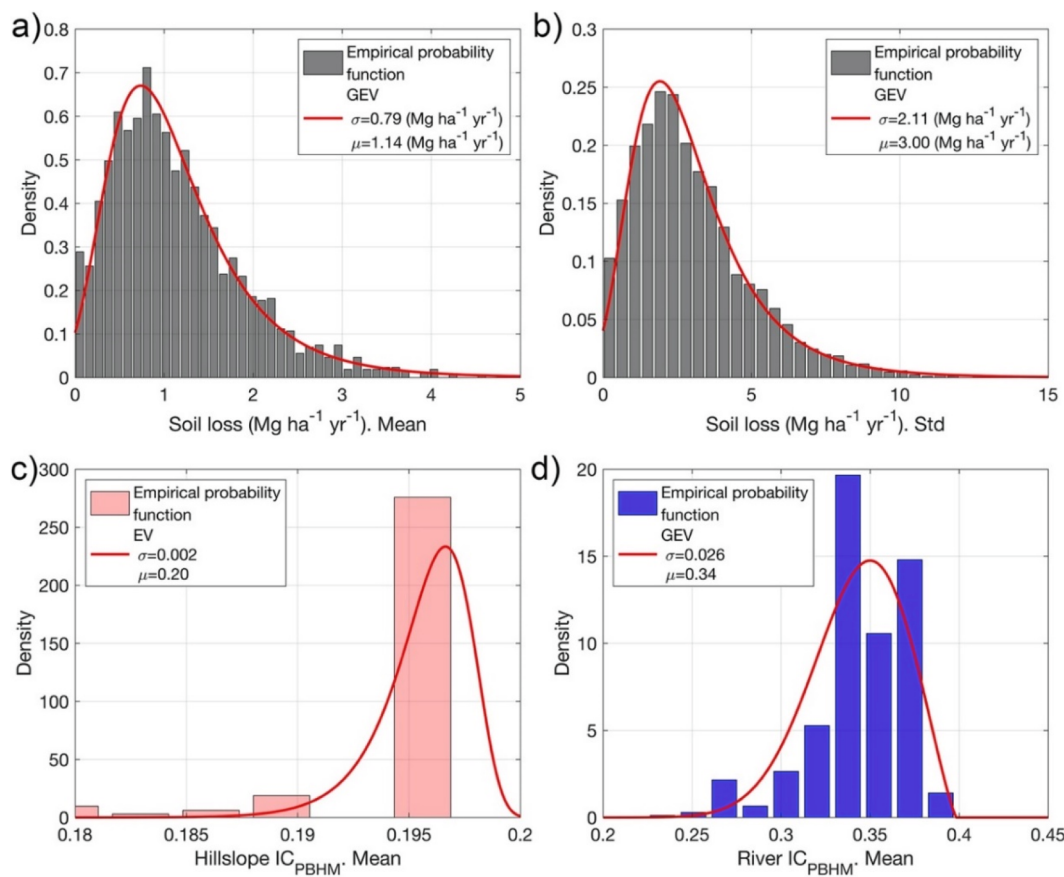


Fig. 13. (a) Mean value of the resulting soil loss map ($Mg\ ha^{-1}\ yr^{-1}$). (b) Standard deviation of the resulting soil loss map ($Mg\ ha^{-1}\ yr^{-1}$). (c) Mean value of the IC_{PBHM} map for hillslopes. (d). Mean value of the map of IC_{PBHM} in rivers.

based on relief and land use and, therefore, between structural and functional sediment connectivity. The spatial distribution of the resulting connectivity indices is similar to the compared methods. However, the results obtained from the event-based approach allow to identify a great variability of sediment connectivity for different precipitation events and hydrological conditions. A constant connectivity value, around 0.19, is observed in headwater hillslope areas, which does not differ for the different events. Connectivity in the remaining part of the hillslopes increases proportionally with the runoff magnitude of the modeled event. These results are comparable to the methodology proposed by Cavalli et al., (2013), although are considerably higher in headwater areas (0.1 vs 0.19). However, the modeled results presented important differences when compared to a landscape factor based on the C-factor as proposed by Borselli et al., (2008), which shows much more spatial variability. In this regard, catchment relief and variability of runoff present similar influence as impedance factors to sediment movement.

From this comparison, structural connectivity, represented by the catchment topography, dominates in determining the general order of magnitude of connectivity indexes. On the other hand, features affecting functional connectivity, such as soil infiltration and erosion rates, control variations of sediment connectivity between events. From these results it could be argued that hydrological processes could greatly modify sediment connectivity, especially within hillslopes. Furthermore, sediment connectivity appears to be controlled by parameters related to water and sediment flow (riverbed roughness, rill erodibility and particle diameter) rather than by flow-independent factors such as vegetation cover and interrill erodibility.

The results are however subject to large sources of uncertainty mainly related to the limitations of model calibration of erosive rates at

the event scale, the erosion and transport processes considered, as well as the magnitude and spatial distribution of runoff, only contrasted at the basin outlet. These limitations highlight the need for greater and better distributed monitoring of water and sediment fluxes throughout the basin. In addition, geomorphological criteria, such as the separation between hillslope and channel areas in modeling tasks, can considerably affect the connectivity value of the sediment, especially along the fluvial system. In this regard, the results and limitations found in this research highlight the important future challenges in a more dynamic understanding of sediment connectivity in our basins.

Declaration of Competing Interest

The authors declare that they have no known competing financial interests or personal relationships that could have appeared to influence the work reported in this paper.

Acknowledgements

This work was financed by ERDF/Spanish Ministry of Science, Innovation and Universities-State Research Agency (AEI)/Project CGL2017-84625-C2-1-R (CCAMICEM); State Program for Research, Development and Innovation focused on the Challenges of Society. The authors would like to thank the anonymous reviewers, whose comments have greatly improved the quality of this paper. We also would like to extend our thanks to the State Meteorology Agency (AEMET), in Spain, for providing meteorological data, and to the Segura River Hydrographic Confederation Center (SHC), Government of Spain, for its collaboration.

Data availability statement

The data sets used and/or analyzed during the current study are available from the corresponding author on reasonable request.

References

- Arcement, G.J., Schneider, V.R., 1989. Guide to selecting Manning's roughness coefficients for natural channels and floodplains. United States Geological Survey Water Supply Paper. U.S. Department of the Interior.
- Baartman, J.E.M., Nunes, J.P., Masselink, R., Darboux, F., Bielders, C., Degré, A., Cantreul, V., Cerdan, O., Grangeon, T., Fiener, P., Wilken, F., Schindewolf, M., Wainwright, J., 2020. What do models tell us about water and sediment connectivity? *Geomorphology* 367, 107300. <https://doi.org/10.1016/j.geomorph.2020.107300>.
- Borselli, L., Cassi, P., Torri, D., 2008. Prolegomena to sediment and flow connectivity in the landscape: a GIS and field numerical assessment. *Catena* 75 (3), 268–277.
- Bracken, L.J., Turnbull, L., Wainwright, J., Bogaart, P., 2015. Sediment connectivity: a framework for understanding sediment transfer at multiple scales. *Earth Surf. Proc. Land.* 40 (2), 177–188.
- Brardinoni, F., 2018. Indices of sediment connectivity: Opportunities, challenges and limitations. *Earth-Sci. Rev.* 187, 77–108. <https://doi.org/10.1016/j.earscirev.2018.08.004>.
- Cavalli, M., Trevisani, S., Comiti, F., Marchi, L., 2013. Geomorphometric assessment of spatial sediment connectivity in small Alpine catchments. *Geomorphology* 188, 31–41.
- CNIG, 2020. Data from the Digital Elevation Model (DEM), retrieved from <http://centrodedescargas.cnig.es/CentroDescargas/index.jsp> in January 2020.
- Conesa-García, C., 1995. Torrential flow frequency and morphological adjustments of ephemeral channels in south-east Spain. In: E.J. Hickin (Ed.), *River Geomorphology* (pp. 169–192). Chichester: John Wiley and Sons.
- Coulthard, T.J., Van De Wiel, M.J., 2017. Modelling long term basin scale sediment connectivity, driven by spatial land use changes. *Geomorphology* 277, 265–281.
- Courant, R., Friedrichs, K., Lewy, H., 1928. Über die partiellen Differenzengleichungen der mathematischen Physik. *Math. Ann.* 100 (1), 32–74.
- Cossart, É., Fressard, M., 2017. Assessment of structural sediment connectivity within catchments: insights from graph theory. *Earth Surf. Dyn.* 5 (2), 253–268.
- CLC, 2018. Corine Land Cover, European Union, Copernicus Land Monitoring Service. European Environment Agency (EEA). retrieved from <https://land.copernicus.eu/pan-european/corine-land-cover> on January 2020.
- Dirección General de Medio Natural y Política Forestal, 2007. *Inventario Nacional de Erosión de Suelos 2002-2012. Región de Murcia*. Murcia. Ministerio de Medio Ambiente Rural y Marino, Madrid.
- Ekhout, J.P.C., Hunink, J.E., Terink, W., de Vente, J., 2018. Why increased extreme precipitation under climate change negatively affects water security. *Hydrolog. Earth Syst. Sci.* 22 (11), 5935–5946. <https://doi.org/10.5194/hess-22-5935-2018>.
- Ekhout, J.P.C., Boix-Fayos, C., Pérez-Cutillas, P., de Vente, J., 2020. The impact of reservoir construction and changes in land use and climate on ecosystem services in a large Mediterranean catchment. *J. Hydrol.* 590, 125208. <https://doi.org/10.1016/j.jhydrol.2020.125208>.
- Engman, E.T., 1986. Roughness coefficients for routing surface run-off. *J. Irrig. Drain. Eng.* 112 (1), 39–53.
- Esteves, M., Faucher, X., Galle, S., Vauclin, M., 2000. Overland flow and infiltration modelling for small plots during unsteady rain: numerical results versus observed values. *J. Hydrol.* 228 (3–4), 265–282.
- Ferro, V., 1998. Evaluating overland flow sediment transport capacity. *Hydrolog. Process.* 12 (12), 1895–1910.
- Foster, G., Flanagan, D., Nearing, M., Lane, L., Risso, L., Finkner, S., 1995. Hillslope Erosion Component. WEPP, vols. 11(1) USDA-Water Erosion Prediction Project.
- Fortugno, D., Boix-Fayos, C., Bombino, G., Denisi, P., Quiñonero Rubio, J.M., Tamburino, V., Zema, D.A., 2017. Adjustments in channel morphology due to land-use changes and check dam installation in mountain torrents of Calabria (southern Italy). *Earth Surf. Proc. Land.* 42 (14), 2469–2483.
- Fryirs, K., Brierley, G.J., 2001. Variability in sediment delivery and storage along river courses in Bega catchment, NSW, Australia: implications for geomorphic river recovery. *Geomorphology* 38 (3–4), 237–265.
- Gay, A., Cerdan, O., Mardhel, V., Desmet, M., 2016. Application of an index of sediment connectivity in a lowland area. *J. Soils Sediments* 16 (1), 280–293.
- Gilley, J., Weltz, M., 1995. In: Flanagan, D.C., Nearing, M.A. (Eds.), *Hydraulics of Overland Flow. USDA-water Erosion Prediction Project: Hillslope Profile and Watershed Model Documentation*, NSERL Report 10.
- Green, W., Ampt, G., 1911. Studies on soil physics: I. flow of air and water through soils. *J. Agric. Sci.* 4, 1–24.
- Grindlay, A.L., Zamorano, M., Rodríguez, M.I., Molero, E., Urrea, M.A., 2011. Implementation of the European Water Framework Directive: Integration of hydrological and regional planning at the Segura River Basin, southeast Spain. *Land Use Policy* 28 (1), 242–256.
- Govers, G., 1992. Relationship between discharge, velocity and flow area for rills eroding loose, non-layered materials. *Earth Surf. Proc. Land.* 17 (5), 515–528.
- Harper, S.E., Foster, I.D., Lawler, D.M., Mathers, K.L., McKenzie, M., Petts, G.E., 2017. The complexities of measuring fine sediment accumulation within gravel-bed rivers. *River Res. Appl.* 33 (10), 1575–1584. <https://doi.org/10.1002/rra.3198>.
- Heckmann, T., Cavalli, M., Cerdan, O., Foerster, S., Javaux, M., Lode, E., Smetanová, A., Vericat, D., Brardinoni, F., 2018. Indices of sediment connectivity: opportunities, challenges and limitations. *Earth-Science Reviews* 187, 77–108.
- Hengl, T., Mendes de Jesus, J., Heuvelink, G. B. M., Ruiperez Gonzalez, M., Kilibarda, M., Blagotić, A., Shangguan, W., Wright, M. N., Geng, X., Bauer-Marschallinger, B., Guevara, M. A., Vargas, R., MacMillan, R. A., Batjes, N. H., Leenaars, J. G. B., Ribeiro, E., Wheeler, I., Mantel, S., Kempen, B., 2017. SoilGrids250m: Global gridded soil information based on machine learning, edited by B. Bond-Lamberty. *PLoS One* 12(2), e0169748. <https://doi.org/10.1371/journal.pone.0169748>.
- Hout, R., Maleval, V., Mahe, G., Rouvillac, E., Crouzeville, R., Cerbelaud, F., 2020. UAV and LiDAR Data in the Service of Bank Gully Erosion Measurement in Rambla de Algeciras Lakeshore. *Water* 12 (10), 2748.
- Hooke, J., Sandercock, P., Cammeraat, L.H., Lesschen, J.P., Borselli, L., Torri, D., Navarro-Cano, J.A., 2017. In: *Mechanisms of degradation and identification of connectivity and erosion hotspots*. Springer, Cham, pp. 13–37.
- Jain, M.K., Singh, V.P., 2005. DEM-based modelling of surface runoff using diffusion wave equation. *J. Hydrol.* 302 (1–4), 107–126.
- Jaeger, K. L., Sutfin, N. A., Tooth, S., Michaelides, K., Singer, M., 2017. Geomorphology and sediment regimes of intermittent rivers and ephemeral streams. In: T. Datry, N. Bonada, A.J. Boulton (Eds.), *Intermittent Rivers and Ephemeral Streams Ecology and Management*, Academic Press (2017), pp. 21–49.
- Kalantari, Z., Lyon, S.W., Jansson, P.-E., Stolte, J., French, H.K., Folkeson, L., Sassner, M., 2015. Modeller subjectivity and calibration impacts on hydrological model applications: An event-based comparison for a road-adjacent catchment in south-east Norway. *Sci. Total Environ.* 502, 315–329.
- Kalantari, Z., Cavalli, M., Cantone, C., Crema, S., Destouni, G., 2017. Flood probability quantification for road infrastructure: data-driven spatial-statistical approach and case study applications. *Sci. Total Environ.* 581–582, 386–398. <https://doi.org/10.1016/j.scitotenv.2016.12.147>.
- Knapen, A., Poesen, J., Govers, G., Gyssels, G., Nachtergaele, J., 2007. Resistance of soils to concentrated flow erosion: A review. *Earth Sci. Rev.* 80 (1–2), 75–109.
- Kim, J., Ivanov, V.Y., 2014. On the non-uniqueness of sediment yield at the catchment scale: The effects of soil antecedent conditions and surface shield. *Water Resour. Res.* 50 (2), 1025–1045.
- Lana-Renault, N., Latron, J., Regués, D., 2007. Streamflow response and water-table dynamics in a sub-Mediterranean research catchment (Central Pyrenees). *J. Hydrol.* 347 (3–4), 497–507.
- Lane, S.N., 2013. 21st century climate change: where has all the geomorphology gone? *Earth Surf. Proc. Land.* 38 (1), 106–110.
- Lane, S.N., Bakker, M., Gabbud, C., Micheletti, N., Saugy, J.-N., 2017. Sediment export, transient landscape response and catchment-scale connectivity following rapid climate warming and Alpine glacier recession. *Geomorphology* 277, 210–227.
- Larson, W.E., Lindstrom, M.J., Schumacher, T.E., 1997. The role of severe storms in soil erosion: a problem needing consideration. *J. Soil Water Conserv.* 50, 90–95.
- Leopold, L.B., Maddock, T., 1953. *The Hydraulic Geometry of Stream Channels and Some Physiographic Implications*, vol. 252 US Government Printing Office, Washington, D. C.
- Liebenow, M., Elliot, W., Lafren, J., Kohl, K., 1990. Interrill erodibility: collection and analysis of data from cropland soils. *Transactions of the ASAE* 33, 1882–1888.
- Lisenby, P.E., Fryirs, K.A., Thompson, C.J., 2020. River sensitivity and sediment connectivity as tools for assessing future geomorphic channel behavior. *Int. J. River Basin Managem.* 18 (3), 279–293.
- Liu, G., Zhang, Q., Yang, M., 2011. Using 7Be to Trace Temporal Variation of Interrill and Rill Erosion on Slopes. *Procedia Environ. Sci.* 11, 1220–1226.
- López Bermúdez, F., Conesa García, C., Alonso Sarria, F., Belmonte Serrato, F., 2000. La cuenca experimental de Rambla Salada (Murcia): investigaciones hidrogeomorfológicas. *Cuadernos de Investigación Geográfica* 26 (0), 95. <https://doi.org/10.18172/cig.vol26iss010.18172/cig.1065>.
- López-Bermúdez, F., Conesa-García, C., Alonso-Sarria, F., 2002. Floods: magnitude and frequency in ephemeral streams of the Spanish Mediterranean region. *Bull. LJ, Kirkby, MJ (Eds.), Dryland Rivers: Hydrology and Geomorphology of Semi-Arid Channels*, Wiley, Chichester, 329–350.
- Maetens, W., Vanmaercke, M., Poesen, J., Jankauskas, B., Jankauskiene, G., Ionita, I., 2012. Effects of land use on annual runoff and soil loss in Europe and the Mediterranean: A meta-analysis of plot data. *Prog. Phys. Geogr.* 36 (5), 599–653.
- Mancilla, G.A., Chen, S., McCool, D.K., 2005. Rill density prediction and flow velocity distributions on agricultural areas in the pacific northwest. *Soil Tillage Research* 84 (1), 54–66.
- Martínez-Salvador, A., Millares, A., Ekhout, J.P., Conesa-García, C., 2021. Assessment of Streamflow from EURO-CORDEX Regional Climate Simulations in Semi-Arid Catchments Using the SWAT Model. *Sustainability* 13 (13), 7120.
- Masselink, R.J.H., Heckmann, T., Temme, A.J.A.M., Anders, N.S., Gooren, H.P.A., Keesstra, S.D., 2017. A network theory approach for a better understanding of overland flow connectivity. *Hydrolog. Process.* 31 (1), 207–220. <https://doi.org/10.1002/hyp.10993>.
- Medeiros, S.C., Hagen, S.C., Weishampel, J.F., 2012. Comparison of floodplain surface roughness parameters derived from land cover data and field measurements. *J. Hydrol.* 452–453, 139–149.
- Merheb, M., Moussa, R., Abdallah, C., Colin, F., Perrin, C., Baghdadi, N., 2016. Hydrological response characteristics of Mediterranean catchments at different time scales: a meta-analysis. *Hydrolog. Sci. J.* 61 (14), 2520–2539.
- Merritt, W.S., Letcher, R.A., Jakeman, A.J., 2003. A review of erosion and sediment transport models. *Environ. Modell. Software* 18 (8–9), 761–799.
- Messenzehl, K., Hoffmann, T., Dikau, R., 2014. Sediment connectivity in the high-alpine valley of Val Müschausen, Swiss National Park—linking geomorphic field mapping with geomorphometric modelling. *Geomorphology* 221, 215–229.

- Micheletti, N., Lane, S.N., 2016. Water yield and sediment export in small, partially glaciated Alpine watersheds in a warming climate. *Water Resour. Res.* 52 (6), 4924–4943.
- Millares, A., Moñino, A., 2018. Sediment yield and transport process assessment from reservoir monitoring in a semi-arid mountainous river. *Hydrol. Process.* 32 (19), 2990–3005.
- Millares, A., Díez-Minguito, M., Moñino, A., 2019. Evaluating gully effects on modeling erosive responses at basin scale. *Environ. Modell. Software* 111, 61–71.
- Millares, A., Moñino, A., 2020. Hydro-meteorological drivers influencing suspended sediment transport and yield in a semi-arid mountainous basin. *Earth Surf. Proc. Land.* 45 (15), 3791–3807. <https://doi.org/10.1002/esp.5001>.
- Millares, A., Chikh, H.A., Habi, M., Morsli, B., Galve, J.P., Perez-Peña, J.V., Martín-Rosales, W., 2020. Seasonal patterns of suspended sediment load and erosion-transport assessment in a Mediterranean basin. *Hydrol. Sci. J.* 65 (6), 969–983. <https://doi.org/10.1080/02626667.2020.1724294>.
- Moreno-Llorca, R., Vaz, A.S., Herrero, J., Millares, A., Bonet-García, F.J., Alcaraz-Segura, D., 2020. Multi-scale evolution of ecosystem services' supply in Sierra Nevada (Spain): An assessment over the last half-century. *Ecosyst. Serv.* 46, 101204. <https://doi.org/10.1016/j.ecoser.2020.101204>.
- Morgan, R. P. C., 2005. Soil Erosion and Conservation. Blackwell Science Ltd, Malden, USA, 3rd edition.
- Moriasi, D.N., Arnold, J.G., Van Liew, M.W., Bingner, R.L., Harmel, R.D., Veith, T.L., 2007. Model evaluation guidelines for systematic quantification of accuracy in watershed simulations. *Trans. ASABE* 50 (3), 885–900.
- Moriasi, D.N., Gitau, M.W., Pai, N., Daggupati, P., 2015. Hydrologic and water quality models: Performance measures and evaluation criteria. *Trans. ASABE* 58 (6), 1763–1785.
- Najafi, S., Dragovich, D., Heckmann, T., Sadeghi, S.H., 2021. Sediment connectivity concepts and approaches. *Catena* 196, 104880. <https://doi.org/10.1016/j.catena.2020.104880>.
- Nearing, M., Foster, G., Lane, L., Finkner, S., 1989. A process-based soil erosion model for USDA-Water Erosion Prediction Project technology. *Trans. ASAE* 32, 1587–1593.
- Niu, Y., Gao, Z., Li, Y., Luo, K.E., 2019. Effect of rock fragment content on erosion processes of disturbed soil accumulation under field scouring conditions. *J. Soils Sedim.* 19 (4), 1708–1723.
- Panagos, P., Borrelli, P., Meusburger, C., Alewell, C., Lugato, E., Montanarella, L., 2015. Estimating the soil erosion cover-management factor at European scale. *Land Use policy journal* 48C, 38–50. <https://doi.org/10.1016/j.landusepol.2015.05.021>.
- Persichillo, M.G., Bordoni, M., Cavalli, M., Crema, S., Meisina, C., 2018. The role of human activities on sediment connectivity of shallow landslides. *Catena* 160, 261–274. <https://doi.org/10.1016/j.landusepol.2015.05.021>.
- Rainato, R., Picco, L., Cavalli, M., Mao, L., Neverman, A.J., Tarolli, P., 2018. Coupling climate conditions, sediment sources and sediment transport in an alpine basin. *Land Degrad. Dev.* 29 (4), 1154–1166.
- Rawls, W., Brakensiek, D., 1983. A procedure to predict Green and Ampt infiltration parameters. In: Proceedings of the American Society of Agricultural Engineers Conference on Advances in Infiltration, pp. 102–112.
- Renard, K.G., Foster, G.R., Weesies, G.A., Porter, J.P., 1991. RUSLE: Revised Universal Soil Loss Equation. *J. Soil Water Conserv.* 46, 30–33.
- Rojo, J., Sánchez-Fuster, M.C., 1996. Red de estaciones experimentales de seguimiento y evaluación de la erosión y desertificación RESEL. Proyecto LUCDEME. Dirección General de Conservación de la Naturaleza. Ministerio de Medio Ambiente. Madrid, 121 pp.
- Romero Diaz, M.A., López Bermúdez, F., Cabezas, F., 1992. Erosion and fluvial sedimentation in the River Segura Basin (Spain). *J. Soil Sci. Hydrol. Geomorphol.* 19 (3-4), 379–392.
- Romero, C.C., Stroosnijder, L., Baigorria, G.A., 2007. Interrill and rill erodibility in the northern Andean Highlands. *Catena* 70 (2), 105–113.
- Saffarpour, S., Western, A.W., Adams, R., McDonnell, J.J., 2016. Multiple runoff processes 453 and multiple thresholds control agricultural runoff generation. *Hydrolog. Earth Syst. Sci.* 20, 4525–4545.
- Saxton, K.E., Rawls, W.J., 2006. Soil water characteristic estimates by texture and organic matter for hydrologic solutions. *Soil Sci. Soc. Am. J.* 70 (5), 1569–1578.
- Shirazi, M.A., Boersma, L., 1984. A unifying quantitative analysis of soil texture. *Soil Sci. Soc. Am. J.* 48 (1), 142–147.
- Simon, A., Curini, A., Darby, S.E., Langendoen, E.J., 2000. Bank and near-bank processes in an incised channel. *Geomorphology* 35 (3-4), 193–217.
- Smetanová, A., Le Bissonnais, Y., Raclot, D., Pedro Nunes, J., Licciardello, F., Le Bouteiller, C., Latron, J., Rodríguez Caballero, E., Mathys, N., Klotz, S., Mekki, I., Gallart, F., Solé Benet, A., Pérez Gallego, N., Andreux, P., Moussa, R., Planchon, O., Santos, J.M., Alshihabi, O., Chikhaoui, M., Follain, S., 2018a. Temporal variability and time compression of sediment yield in small Mediterranean catchments: impacts for land and water management. *Soil Use Manage* 34 (3), 388–403. <https://doi.org/10.1111/sum.12437>.
- Smetanová, A., Paton, E.N., Maynard, C., Tindale, S., Fernández-Getino, A.P., Marquéus Pérez, M.J., Bracken, L., Le Bissonnais, Y., Keesstra, S.D., 2018b. Stakeholders' perception of the relevance of water and sediment connectivity in water and land management. *Land Degrad. Dev.* 29 (6), 1833–1844.
- Soilgrids, 2020. Soil Profile Database from World Soil Information Service (WoSIS), retrieved from <https://soilgrids.org/> in January 2020.
- Thoman, R.W., Niezgoda, S.L., 2008. Determining erodibility, critical shear stress, and allowable discharge estimates for cohesive channels: Case study in the Powder River basin of Wyoming. *J. Hydraul. Eng.* 134 (12), 1677–1687.
- Thomas, J.T., Iverson, N.R., Burkart, M.R., Kramer, L.A., 2004. Long-term growth of a valley-bottom gully, western Iowa. *Earth Surf. Proc. Land.* 29 (8), 995–1009.
- Turnbull, L., Hütt, M.-T., Ioannides, A.A., Kininmonth, S., Poepll, R., Tockner, K., Bracken, L.J., Keesstra, S., Liu, L., Masselink, R., Parsons, A.J., 2018. Connectivity and complex systems: learning from a multidisciplinary perspective. *Appl. Netw. Sci.* 3 (1) <https://doi.org/10.1007/s41109-018-0067-2>.
- Turnbull, L., Wainwright, J., 2019. From structure to function: Understanding shrub encroachment in drylands using hydrological and sediment connectivity. *Ecol. Ind.* 98, 608–618.
- van Griensven, A.V., Meixner, T., Grunwald, S., Bishop, T., Diluzio, M., Srinivasan, R., 2006. A global sensitivity analysis tool for the parameters of multi-variable catchment models. *J. Hydrol.* 324 (1–4), 10–23.
- Wainwright, J., Turnbull, L., Ibrahim, T.G., Lexartza-Artza, I., Thornton, S.F., Brazier, R. E., 2011. Linking environmental regimes, space and time: Interpretations of structural and functional connectivity. *Geomorphology* 126 (3–4), 387–404.
- Weltz, M.A., Arslan, A.B., Lane, L.J., 1992. Hydraulic roughness coefficients for native rangelands. *J. Irrig. Drain. Eng.* 118 (5), 776–790.
- Xiao, H., Liu, G., Liu, P., Zheng, F., Zhang, J., Hu, F., 2017. Developing equations to explore relationships between aggregate stability and erodibility in Ultisols of subtropical China. *Catena* 157, 279–285.
- Yalin, M.S., 1963. An expression for bed-load transportation. *J. Hydraulics Division* 89 (3), 221–250.